Analysing UHPFRC beams with the help of ANSYS

ØYSTEIN GRØSTAD   ESPEN SANDBERG

UNIVERSITETET I AGDER

Obligatorisk egenerklæring/gruppeerklæring

Den enkelte student er selv ansvarlig for å sette seg inn i hva som er lovlige hjelpemidler, retningslinjer for bruk av disse og regler om kildebruk. Erklæringen skal bevisstgjøre studentene på deres ansvar og hvilke konsekvenser fusk kan medføre. Manglende erklæring fritar ikke studentene fra sitt ansvar.

1.	Jeg/vi erklærer herved at min/vår besvarelse er mitt/vårt eget arbeid, og at jeg/vi ikke har brukt andre kilder eller har mottatt annen hjelp enn det som er nevnt i besvarelsen.	☒
2.	Jeg/vi erklærer videre at denne besvarelsen: - ikke har vært brukt til annen eksamen ved annen avdeling/universitet/høgskole innenlands eller utenlands. - ikke refererer til andres arbeid uten at det er oppgitt. - ikke refererer til eget tidligere arbeid uten at det er oppgitt. - har alle referansene oppgitt i litteraturlisten. - ikke er en kopi, duplikat eller avskrift av andres arbeid eller besvarelse.	☒
3.	Jeg/vi er kjent med at brudd på ovennevnte er å betrakte som fusk og kan medføre annullering av eksamen og utestengelse fra universiteter og høgskoler i Norge, jf. Universitets- og høgskoleloven §§4-7 og 4-8 og Forskrift om eksamen §§ 31.	☒
4.	Jeg/vi er kjent med at alle innleverte oppgaver kan bli plagiatkontrollert.	☒
5.	Jeg/vi er kjent med at Universitetet i Agder vil behandle alle saker hvor det forligger mistanke om fusk etter høgskolens retningslinjer for behandling av saker om fusk.	☒
6.	Jeg/vi har satt oss inn i regler og retningslinjer i bruk av kilder og referanser på biblioteket sine nettsider.	☒

UNIVERSITETET I AGDER

Publiseringsavtale

Fullmakt til elektronisk publisering av oppgaven

Forfatter(ne) har opphavsrett til oppgaven. Det betyr blant annet enerett til å gjøre verket tilgjengelig for allmennheten (Åndsverkloven. §2).
Alle oppgaver som fyller kriteriene vil bli registrert og publisert i Brage Aura og på UiA sine nettsider med forfatter(ne)s godkjennelse.

Oppgaver som er unntatt offentlighet eller tausehetsbelagt/konfidensiell vil ikke bli publisert.

Jeg/vi gir herved Universitetet i Agder en vederlagsfri rett til å
gjøre oppgaven tilgjengelig for elektronisk publisering: ☒JA   ☐NEI

Er oppgaven båndlagt (konfidensiell)?   ☐JA   ☒NEI
 (Båndleggingsavtale må fylles ut)
   - Hvis ja:
Kan oppgaven publiseres når båndleggingsperioden er over?   ☐JA   ☐NEI

Er oppgaven unntatt offentlighet?   ☐JA   ☒NEI
(inneholder taushetsbelagt informasjon. Jfr. Offl. §13/Fvl. §13)

Publiseringsavtale

Preface

This thesis is written at the department of Engineering Sciences at University of Agder, spring 2018.

The goal of this thesis is to get to know UHPFRC better and to investigate if and how the already existing material model for concrete in ANSYS is possible to use for UHPFRC. Additional knowledge on use of FEA software ANSYS is a positive side-effect of this thesis.

We wanted a better understanding of concrete technology and UHPFRC, and to examine different applications for this material. Research on UHPFRC at University of Agder is high priority, and they are one of the leading institutions on this topic in Norway. There is a starting interest of UHPFRC in the industry, and we think it's just a matter of time before UHPFRC is used in structural design.

The thesis is written in English although this isn't our first language. The reason for this is that much of the information about UHPFRC and related subjects are written in English. This way we keep the precision of the terminology in the literature which may be lost if translated poorly.

We will take this opportunity to thank our supervisors at University of Agder, Rein Terje Thorstensen and Ph.D. candidate Ingrid Lande Larsen for their guidance and professional insight.

We would also like to express our gratitude towards our supervisor at Rambøll, Simen Rindebakken for insight into what the industry needs to start using UHPFRC. And, of course, for valuable feedback and discussion of academic challenges regarding our thesis.

A big thank you to Katalin Vertes for all the help with ANSYS and general guidance through our project period.

We also thank Paul Ragnar Svennevig, Anette Heimdal and our fellow M.SC. and B.Sc. students for much appreciated feedback and discussions through the entire project period.

And last, but not least, we thank our fellow students Piotr Stanislawski, Svava Iselin Idarsdottir and Tonje Schjelderup for proffesional collaboration across M.Sc. projects.

Øystein Grøstad   Espen Sandberg

Grimstad, 31.mai 2018

Summary

This Master thesis is about analysis of Ultra-high performance fibre reinforced concrete (UHPFRC) beams with the help of the Finite Element Analysis software ANSYS. The research question and the operational questions are:

How can we analyse UHPFRC beams with the help of ANSYS?

       How does the built in concrete material model in ANSYS work?

       How can the concrete material model in ANSYS simulate behaviour of UHPFRC beams?

The approach used to answer the questions is based on the hypothetico-deductive method. Hypotheses are built from the theoretical framework and tested in ANSYS. The results from the tests are used to refine the theory, the hypotheses and the tests.

The concrete material model in ANSYS is based on K. J. William and E. P. Warnke's 5-parameter constitutive model for triaxial behaviour of concrete. This theory is naturally central to the work in this thesis.

The results from the tests in ANSYS show that the concrete model can predict the behaviour of relatively small UHPFRC beams with flexural- and shear reinforcement. If the beams are without reinforcement, the model cannot accurately predict the behaviour of the material.

By combining the Drucker-Prager plasticity model to the concrete model in ANSYS, the behaviour improved. To further increase the accuracy of the models a more sophisticated hardening rule is needed. The concrete material model in ANSYS is found to be too inflexible in this regard.

Table of contents

1 Introduction

UHPFRC contains the same constituents as concrete and behaves in the same manner from an overarching point of view. It generally contains larger fractions of cement, pozzolans/admixtures and fine aggregates compared to normal concrete. This leads to a higher amount of cement paste, denser particle packing and a discontinuous pore structure. Thus, resulting in a strong and durable, yet more brittle concrete. Small steel fibres are included in the mix to compensate for this brittle behaviour.

It's a relatively new material with ongoing research to find connections between the material's composition, mechanical properties, structural behaviour and design rules. Research and laboratory tests will get us closer to determine how to implement UHPFRC for commercial use. The industry has shown increasing interest in UHPFRC, and this contributes to faster progress on the development.

Through our contact with Rambøll we were able to get a picture of what the industry needs to use UHPFRC in Norway. They need documentation on how the material behave when exposed to different loading conditions, fire and freeze-thaw cycles. Effective tools for analysis and design of structures are crucial for the implementation of UHPFRC. Finite element analysis (FEA) software is usually what they depend on, and valid material models for accurate simulation of UHPFRC must be developed.

Research and practical experience for about 2000 years has provided us with good material models to simulate normal concrete behaviour. Due to obvious similarities between concrete and UHPFRC it would be fair to assume that these models, to some extent, could be used for UHPFRC as well. At least the models can be used as a basis for material behaviour and then adjusted for UHPFRC. This requires knowledge on how the material models for concrete work, and how they are built.

William-Warnke model, Drucker-Prager- and Rankine yield criterion are such models. These are mathematical models developed to predict material behaviour dependent on the input parameters. Crack initiation and propagation can be predicted by these models. After cracking, the material behaves in a non-linear manner.

When designing and analysing structural components with FEA there are several levels of complexity, depending on the task at hand and what results you're looking for. The choice of material models and element types are essential to acquire adequate results. For a simplified first analysis one can use e.g. a linear elastic material model in combination with design standards and design guides. For a more in-depth analysis it is necessary to address the non-linear behaviour of the material.

This behaviour is critical to simulate post-yield behaviour and how failure occurs. For the William-Warnke based concrete model in ANSYS, post-yield is when the concrete starts to crack and how cracks may propagate. To determine a correct development of crack patterns and fracture, it is crucial to understand how stresses are distributed in the structure.

This Master thesis will address these challenges and bring us a step closer to how we model the behaviour of UHPFRC in FEA.

2 Societal perspective on use of UHPFRC

Concrete has been essential for developing today's society. Our modern society is built and relies on technical possibilities emerged from the invention of cement, concrete and steel-reinforced concrete. Continuous research and development has increased its use and application up until present time. Rebuilding after World War 2 marked the increased use of concrete. Devastating city-fires in 18th-,19th-, and 20th century lead government to condemn timber constructions in the cities, thus escalating the use of concrete. These events contributed to it probably being the most preferred construction material in modern day.

Sustainable and environmentally friendly building materials combined with effective and safe building are the goal and scope of the future. This goal keeps developing our construction materials and their application. UHPFRC is a natural development of concrete with better strength and durability. Its strength is far better than normal concrete due to more cement in the mix. Better durability is achieved by adding a larger fraction of fine aggregates in the mix. Addition of a larger fraction of fine aggregates leads to denser particle packing and a discontinuous pore structure.

Adding more cement to the mix is negative from an environmentally perspective, due to large CO_2 emissions associated with cement production. However, addition of waste- and by-products from other industries is common these days. Waste- and by-products like microsilica, fly ash and blast furnace slag etc. substitutes some of the cement. Research is ongoing in these fields to see how we best can take advantage of these by-products to reduce CO_2 emissions from the concrete industry. By using UHPFRC in an effective manner it's possible to reduce necessary volume for a structure compared to normal concrete. [1] Taking this into account the total use of cement may not increase that much.

Increased cement in the mix gives a proportionally less use of aggregates. Natural occurrence of rounded aggregates is decreasing and, in some countries, becoming scarce. This scarceness is gradually compensated by adding crushed rock. Crushing rocks is energy demanding and therefore contributes to increased CO_2 emissions. Mechanically crushed rock as aggregate is seemingly more challenging to use for concrete purposes. Comprehensive and energy demanding tests is a necessity to verify its performance for concrete purposes. Generally, studies prove natural aggregates perform better than crushed aggregates. [2]

As mentioned earlier, UHPFRC is a strong and durable material. Durability is essential and is given more focus recently. Considering its significantly better durability, it's from an environmentally perspective possible to justify the mix-proportions of UHPFRC. At least when considering necessary future inspections and repairs included in a life-cycle analysis of the structure.

Primary structures like bridges, hospitals, skyscrapers, quays etc. should be made of durable materials. Due to these structures being exposed to severe environmental- and loading conditions, UHPFRC would be beneficial. From a more technical point of view, UHPFRC allows constructions that is not rationally feasible with use of normal concrete and other materials. Examples are bridges with long spans, constraints on structure heights and possibilities for extra supports. If we include prestressing actions the range of possibilities increases even further.

Generally, for all structures, documentation proving safety of use and economical- and ecological efficiency must be provided. This usually means thorough and exhaustive structural evaluations and material tests in laboratories. Some leeway can be given if an effective quality control system is implemented at the production plant and the design office. The quality control systems are usually built upon criteria set by standards and ETAs based on national laws and regulations.

Recently, a French appendix [3] to Eurocode 2 [4] and an accompanying production standard [5] for UHPFRC has been published. These standards are a natural result of many years of scientific work. Unfortunately, they are cumbersome to use, and this is probably one of the reasons why we don't use UHPFRC yet. Scepticism from concrete production plants to invest in new silos and restructure their production line and control routines is also a major factor. This scepticism is relatable as most contractors are unwilling to do pilot-projects to get to know the material. They are unwillingly due to cumbersome design standards and presently not an appendix for Norwegian conditions.

These uncertainties are what prevents the development of UHPFRC. Another drawback is that concrete can be cast in-situ in many different shapes, while UHPFRC currently should be produced in a controlled environment to guarantee performance and safety of use.

The challenge is to establish safe and effective design guides and regulations. Proper engineering routines and tools must be implemented for further development and utilization of UHPFRC. However, much work remains to adapt a standard on the material for Norwegian conditions. Indeed, the industry has shown a growing interest of UHPFRC, considering new applications and increased focus on environmentally friendly and effective building.

3 Theory and literature review

The presented theory is what we use for our understanding of the occurring phenomena of UHPFRC in different stress states. The first part is an overview of stresses and invariants. This is needed to understand the more complicated theories later in this chapter.

3.1 Principal stresses, hydrostatic pressure, deviatoric stresses and invariants

Consider an element of a load-bearing structure. This element can be subjected to stresses in any direction. These stresses are commonly represented by a 2nd order tensor which looks like this in three-dimensional space:
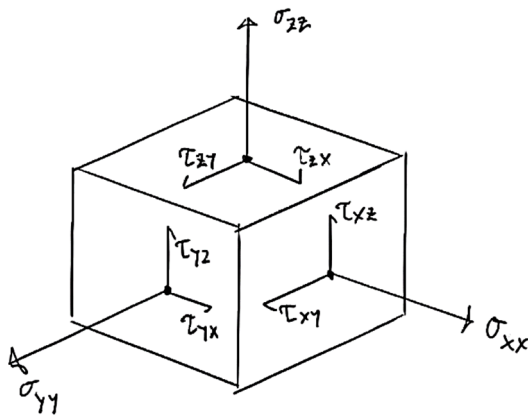
Figure 3.1 Stress Tensor

The tensor can be represented by a symmetrical matrix:

$$A = \begin{bmatrix} \sigma_{xx} & \tau_{xy} & \tau_{xz} \\ & \sigma_{yy} & \tau_{yz} \\ & & \sigma_{zz} \end{bmatrix}$$

The principal stresses of the tensor are the eigenvalues of the matrix and can be found like this:

$$det(A - \sigma I) = 0$$

Where I is the identity matrix

The principal stresses are ordered by descending magnitude and defined so that a positive value is tensile stress.

$$\sigma_1 \geq \sigma_2 \geq \sigma_3$$

These stresses form the principal stress tensor which is equal to the stress tensor in describing the stress state of the element.

4

Below is the tensor in three-dimensional space:
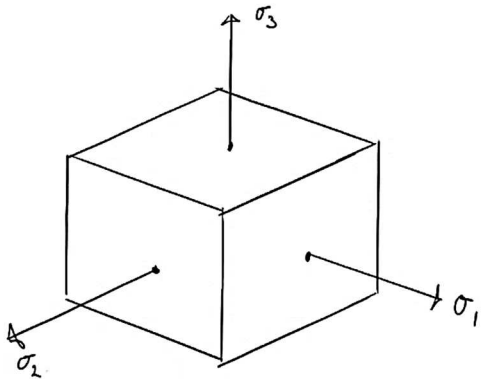
Figure 3.2 Principal Stress Tensor

This tensor can also be described by a symmetrical matrix:

$$\boldsymbol{\sigma} = \begin{bmatrix} \sigma_1 & 0 & 0 \\ & \sigma_2 & 0 \\ & & \sigma_3 \end{bmatrix}$$

Stresses consists of one hydrostatic pressure component and one deviatoric stress component

$$\sigma = \sigma_h + \sigma_d$$

The hydrostatic pressure is the part of the stress tensor that changes the volume of the element and is defined as the average of the principal stresses:

$$\sigma_h = \frac{(\sigma_1 + \sigma_2 + \sigma_3)}{3}$$

The deviatoric stresses are the part of the stress tensor that only distorts the shape of the element. This implies a connection to shear stresses. The deviatoric stresses are found by subtracting the hydrostatic pressure from all the principal stresses.

$$\boldsymbol{\sigma_d} = \begin{bmatrix} \sigma_1 - \sigma_h & 0 & 0 \\ 0 & \sigma_2 - \sigma_h & 0 \\ 0 & 0 & \sigma_3 - \sigma_h \end{bmatrix}$$

The stress invariants are defined as follows:

$$I_1 = \sigma_1 + \sigma_2 + \sigma_3$$
$$I_2 = \sigma_1 \cdot \sigma_2 + \sigma_2 \cdot \sigma_3 + \sigma_1 \cdot \sigma_3$$
$$I_3 = \sigma_1 \cdot \sigma_2 \cdot \sigma_3$$

These three are found from the principal stress tensor. The deviatoric stress invariants are calculated the same way from the deviatoric stress tensor. Often it can be beneficial to express the deviatoric stress invariants by the stress invariants:

$$J_1 = 0$$
$$J_2 = \frac{1}{3} \cdot I_1^2 - I_2$$
$$J_3 = \frac{2}{27} \cdot I_1^3 - \frac{1}{3} \cdot I_1 \cdot I_2 + I_3$$

These are all called invariants because they are independent of rotations of the stress tensor. Both this and the formulas given above imply that the invariants are the same for the stress tensor and the principal stress tensor.

3.2 Material parameters used in this study

3.2.1 Characteristics of the uniaxial stress-strain diagram for UHPFRC in compression

These types of diagrams are effective tools for understanding behaviour of UHPFRC.

The curve starts at an unstressed and unstrained state in origin of the diagram. Increasing compressive stress moves the curve. A given point on the curve will tell the actual compressive stress in relation to strain in the material at this point.

The curve is linear until it reaches the Limit of Proportionality (LoP). This is where the first cracks start to form on a microscopic level. These cracks will not yet damage the structural integrity of the material. Further up the curve we reach the yield point. This point is where the cracks starts to permanently damage the UHPFRC.

After yield we move to a plastic behaviour which permanently deforms the UHPFRC. This plastic behaviour will usually either soften or harden the UHPFRC depending on the characteristics of the fibre-reinforcement. For non fibre-reinforced UHPC the strain length between yield point and failure is shorter compared to normal concrete, thus showing it's more brittle.
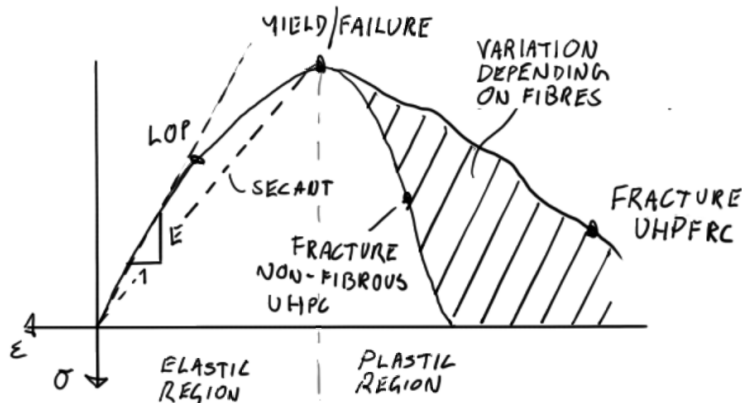

Figure 3.3   Sketch of UHPFRC stress/strain diagram with strain softening post-yield behaviour

3.2.1 E-modulus

We will use a formula for the E-modulus from the research of Ma et al. [6]. They state UHPFRC contains higher amounts of cement paste and will have a lower relative E-modulus when compared to normal concrete.

The E-modulus formula is suited for UHPFRC's with low amount of coarse aggregates and strengths above 150 MPa. Our case uses a strength of 135 MPa. We're not seeking an exact solution of our beams, but if it's possible to predict their behaviour. In this regard this approximation is satisfactory.

$$E = 19000 \left(\frac{f_c}{10}\right)^{\frac{1}{3}} \tag{3.1}$$

The pre-crack behaviour of UHPFRC is nearly linear all the way up to the yield stress. A different scenario is when significant post-crack hardening behaviour is observed. In this case a secant modulus spanning from origin to the yield stress point can be an efficient way of dealing with this.

3.2.2 Tensile strength

UHPFRC has significant tensile strength. An accurate prediction is difficult because of fibre and the many variations of mix designs. Graybeal [7] suggests the following relation to compressive strength which we will use as a baseline in this study.

$$f_t = 0.65 \cdot \sqrt{f_c} \tag{3.2}$$

3.2.3 Poisson's Ratio

In the "State of the art report" [8] from Federal Highway Administration is a table showing six values for Poisson's ratio of UHPC. These are determined by six different researchers, and they are approximately 0.2. We use this value for our tests in ANSYS.

3.3 Failure mechanisms and strength in UHPFRC

The main reasons for failure in concrete and UHPFRC are tensile stresses. These can be direct tensile stresses or tensile stresses resulting from transversal dilation of a concrete element under compression. The tensile stresses will, at increasing magnitudes, cause cracks to propagate and will ultimately break the cohesion of the concrete.
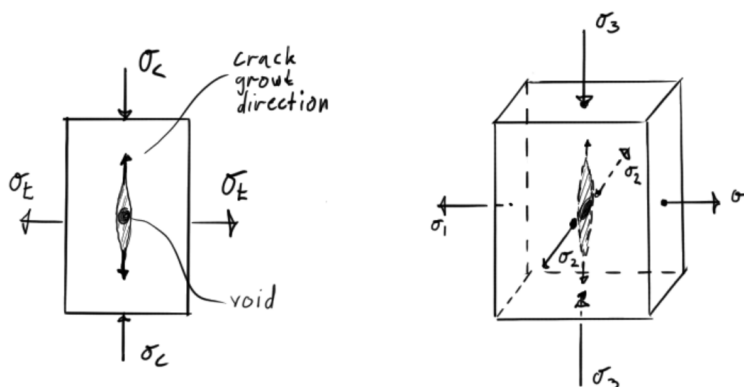

Figure 3.4 Concept of cracking in concrete

Intuitively, if the tensile stresses are hindered, the crack may stop growing. This can happen in two ways; by adding physical confining objects like reinforcement or fibre inside the concrete, or if compressive stresses are applied to the sides. In either case one should suspect that the compressive strength increases. This holds true if the concrete has confining stresses in both σ_1- and σ_2-directions. The concrete is now defined as being in a triaxial compressive stress state, i.e. $0 \geq \sigma_1 \geq \sigma_2 \geq \sigma_3$.

The case of UHPFRC in biaxial compression, i.e. $\sigma_1 > 0 \geq \sigma_2 \geq \sigma_3$, is particularly interesting. Researchers have investigated and performed tests on concrete under biaxial compression [9]. The knowledge drawn from the reports are conceptualised in the figure below:
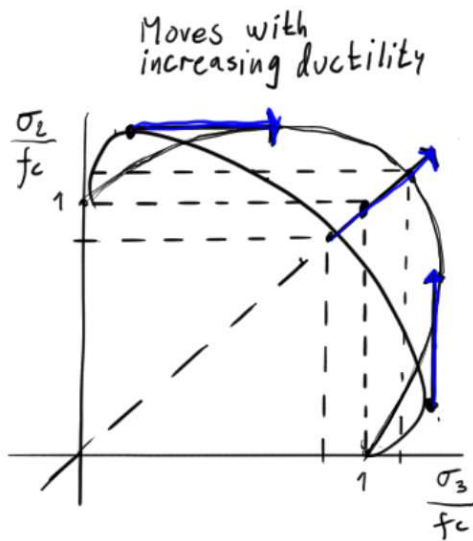

Figure 3.5 Concept sketch of differences in biaxial compressive strength for concretes with increasing ductility

The reduction in biaxial compressive strength for higher strength concrete is attributed to the decrease in ductility. This is interesting for UHPC. Without steel fibre reinforcement, UHPC behaves very brittle in failure and one can expect lower relative strength in biaxial compression. With steel fibres in the mix it is possible to assume a behavior more akin to normal concrete with significant increase in biaxial strength.

On a side note, this effect is partially covered in EC2 6.5.2 [4], where it is stated that the biaxial compressive strength can be increased, but no argument is made as to how much.

3.4 Steel fibres and their efficiency
This sub-chapter is based on the doctoral thesis by Elena Vidal Sarmiento [10], and presented as an overview of the complexities related to fibre reinforcement of concrete. This is a summary of our interpretation of the theory presented by her. Her thesis considers normal concrete, but the same approach is valid for UHPFRC as fibres contributes in the same way.

A fibre efficiency factor can be calculated to determine how addition of fibre-reinforcement contributes to the mechanical performance of UHPFRC. The fibre efficiency factor is defined by fibre orientation and local fibre volume fraction. These two parameters are yet again influenced by variables like rheological properties, casting procedure, fibre properties and mould geometry.

The process of determining the fibre efficiency factor is cumbersome and falls outside the scope of this study.

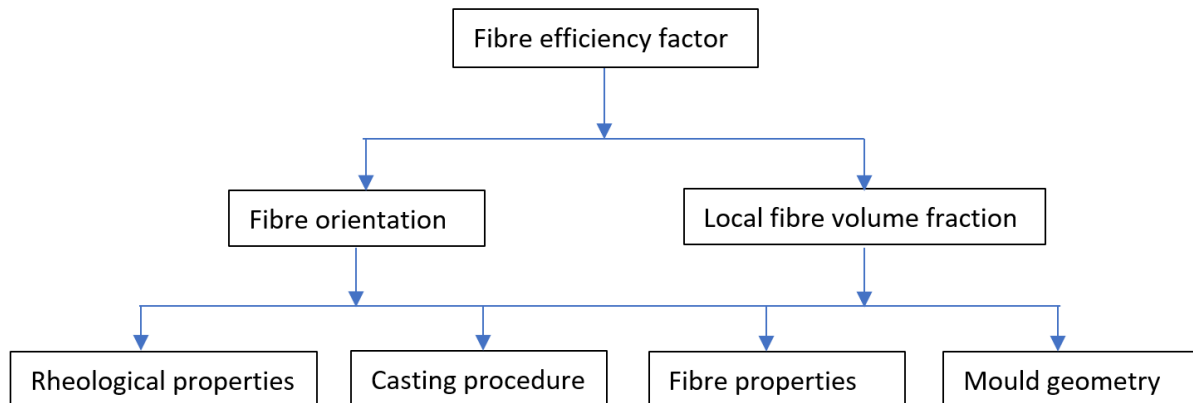This flow chart presents different variables influencing the fibre efficiency factor:

Figure 3.6 Flow chart of fibre efficiency factor

Yield stress is determined as the minimum stress needed for concrete flow to occur. Due to lower stresses for more flowable concrete the more of the fibres will be affected by flow induced orientation. This introduces more anisotropic fibre orientation for more flowable concrete.

Flow of concrete is also influenced by shear stresses occurring under casting. Shear stresses during flow influence the flow velocity profile. Casting method, geometry of the mould and wall effect also influences this flow velocity profile. Due to frictional restraint of the walls in the formwork a variation of the flow velocity will occur and affect the fibre to some degree. This may also affect their orientation. To what degree this affects fibre orientation depends on the fibre properties.

Fibre is available in a variety of materials and shapes. Depending on material they will have different E-modulus. Variation in E-modulus determines how they strengthen the concrete, if they do so at all. Some fibres do not strengthen the concrete at all but reduce plastic shrinkage cracking and drying shrinkage cracking. Some fibres are thin straight short fibres, and some are thicker and longer with hooked ends.

The relation between length and diameter is important and is named aspect ratio. Aspect ratio is length divided by diameter. Larger aspect ratio and greater volume fraction of fibre is reported to influence the flow of the concrete and show tendencies to ball [10] [11] . When fibres ball together they increase the local volume fraction, but they induce an anisotropic fibre distribution.

Flow and stability of the concrete is important with regards to fibre distribution. Some types of concrete are stable at rest, but they become unstable during flow. This instability is caused by the internal friction and the cohesive forces decreasing between particles and matrix with increasing flow length. This is called gravity-induced particle migration and can lead to segregation of the densest particles, which can include fibres.

Sarmiento [10] reports variation of influence depending on fibre properties. Typically, steel fibres are prone to segregation by this effect. Fibres segregating will induce anisotropic fibre distribution with increased local volume fraction in the lower part.

To determine a fibre efficiency factor the relation between fibre orientation and local volume fraction must be known. Sarmiento [10] states that there are several methods on how to determine these factors. Either by e.g. mechanically count fibres over a sliced cross-section from hardened concrete and use this in a formula to get the fibre orientation, or by CT scanning of the cross-section. Crushing a sliced cross-section piece to separate fibres from concrete is possible to determine local volume fraction.

Differences between test-specimens and full scale structural elements is also reported. All these different variables influencing fibre orientation and local volume fraction complicates the process of finding a correct efficiency factor. Without this efficiency factor it's not possible to determine how fibres contribute to the mechanical performance of UHPFRC.

3.5 Yield criterions

The background for the material models used by ANSYS is explained here. The text presented here is our understanding of the theories and what we need to consider when applying them in ANSYS.

3.5.1 Rankine maximum principal stress theory

This theory was developed in the middle of the nineteenth century by a Scottish engineer named William J.M. Rankine [12]. Originally it was developed for use in soil mechanics but has seen application in many structural engineering fields. The theory states that any material yields when a principal stress reaches maximum tensile strength.

$$\sigma_1 < f_t$$
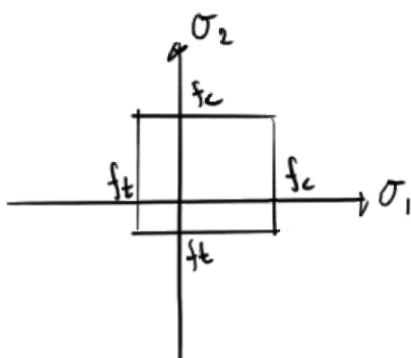
Figure 3.7 Rankine failure envelope for biaxial stress state

This looks quite simple, but the theory behind it is quite advanced. As can be seen from the figure above, the model doesn't consider shear stresses at all. Thus, the model doesn't work that well for metals. For brittle materials, and especially if exposed to tensile stresses, this model can reasonably describe the behaviour. The model does not have a smooth circumference which can lead to computational complexities, e.g. when trying to use differentiation.

3.5.2 Drucker-Prager yield criterion

Daniel C. Drucker and William Prager developed this theory [13] in the middle of the 20th century. To start off, it is well known that the strength of concrete is dependent the hydrostatic pressure. The Drucker-Prager yield criterion takes dependence on hydrostatic pressure into account by modelling the yield surface as a cone, with its "apex" ending in the tensile octant of the principal stress space. The hydrostatic axis is the centerline through the volume and is angled 45° on all three main axes.
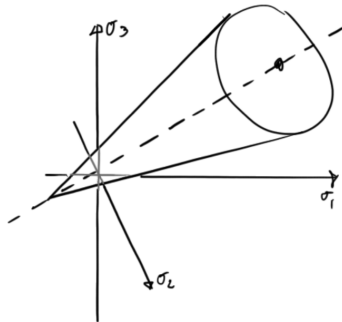

Figure 3.8 Drucker-Prager failure envelope for triaxial stress state
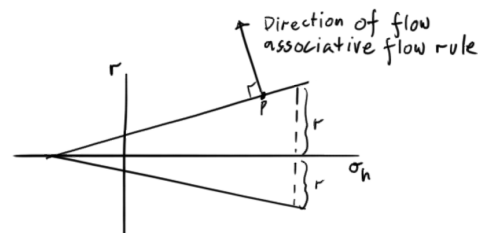
Figure 3.9 Drucker-Prager failure envelope in $\sigma_h - r$ space

For reference, the general form of the failure criterion reads:

$$\boldsymbol{f} = \alpha \cdot I_1 + \sqrt{J_2} = k$$

Like Mohr-Coulomb [14], this theory also depends on defining values for cohesion (c) and frictional angle (θ_f).

These can be calculated through the values on uniaxial compressive- and tensile strength like this:

$$\theta_f = \arcsin\left(\frac{3 \cdot \sqrt{3} \cdot \beta}{2 + \sqrt{3} \cdot \beta}\right) \tag{3.3}$$

$$c = \gamma \cdot \sqrt{3} \cdot \left(\frac{3 - \sin(\theta_f)}{6 \cdot \cos(\theta_f)}\right) \tag{3.4}$$

$$\beta = \frac{f_c - f_t}{\sqrt{3} \cdot (f_c + f_t)} \tag{3.5}$$

$$\gamma = \frac{2 \cdot f_c \cdot f_t}{\sqrt{3} \cdot (f_c + f_t)} \tag{3.6}$$

In addition, a flow rule can be determined through the angle of dilatancy. If this angle is set equal to the friction angle, the flow is associative and directed normal to the yield surface. From the documentation on the model in ANSYS it is stated that setting $\theta_d < \theta_f$ reduces the amount of volumetric dilatancy and implies a non-associative flow rule. The flow rule concept is touched upon later in chapter 3.7.1.

3.5.3 William-Warnke 5-parameter constitutive model for triaxial behavior in concrete

This yield criterion was developed by K. J. William and E. P. Warnke in the 1970's. The criterion is sophisticated and pretends to be general for normal concrete. This is close to true within the normal safety regime for concrete structure design.

The original paper [15] on the model states that concrete yields if

$$f(\sigma_h, \tau_h, \theta) \leq \frac{1}{r(\sigma_h, \theta)} \cdot \frac{\tau_h}{f_c} - 1$$

First off, for comparison with the Drucker-Prager yield criterion, the left-hand side of the above inequality is of the form $f(I_1, J_2, J_3)$. It is expanded by the inclusion of J_3.

$$r(\sigma_h, \theta) = \frac{2 \cdot r_2(r_2^2 - r_1^2) \cdot cos\theta + r_2(2 \cdot r_1 - r_2)\sqrt{4(r_2^2 - r_1^2)cos^2\theta + 5 \cdot r_1 - 4r_1 r_2}}{4(r_2^2 - r_1^2)cos^2\theta + (r_2 - 2r_1)^2}$$

where $r(\sigma_h, \theta)$ is the yield surface of concrete. The component σ_h tells us that this model is dependent on the hydrostatic pressure. This function is large and cumbersome to perform mathematical operations on, but the material model in ANSYS is built on it. Some useful information can be drawn directly from the formula. Other than the lode angle (θ), the function depends on r_1 and r_2. These radii are used to define the geometry of the yield envelope and they include the strength parameters of the concrete.

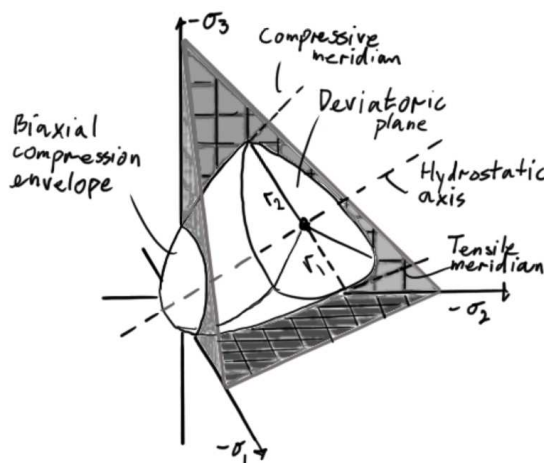It is easier to visualize this in principal stress space.

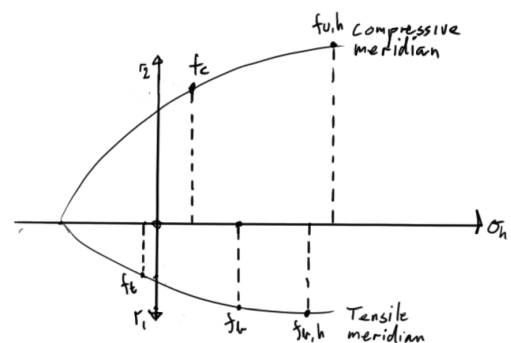*Figure 3.10 William Warnke yield surface in principal stress space*   *Figure 3.11 William-Warnke yield suface in $\sigma_h - r$ space*

At lower stress ranges, concrete exhibits a strong dependence on the hydrostatic pressure. At higher stress ranges, this dependence is not as pronounced.

It is interesting to note that the William-Warnke model degenerates into Drucker-Prager and von Mises when the parameters controlling the radii are set accordingly. More about this can be read in the original paper [15].

At the core, this model is governed by 5 strength parameters

Uniaxial compressive strength f_c
Uniaxial tensile strength f_t
Biaxial compressive strength f_b
Uniaxial compressive strength at hydrostatic pressure $f_{c,h}$
Biaxial compressive strength at hydrostatic pressure $f_{b,h}$

An expected value of hydrostatic stress must be determined for $f_{c,h}$ and $f_{b,h}$

3.6 Drucker's stability postulate

According to Drucker's postulate [16] a material is stable if the yield surface is convex at every point and the direction of plastic strains follow the normality principle. The convexity means that there cannot be any inflection points along the yield surface. The normality principle states that if a normal is constructed to the yield point when the combination of stresses reaches yielding, the strains in each direction is proportional to the stress components of the normal. The implications of this is that if the work done by an incremental stress is non-negative, the material is stable. Below is a sketch in stress/strain space:
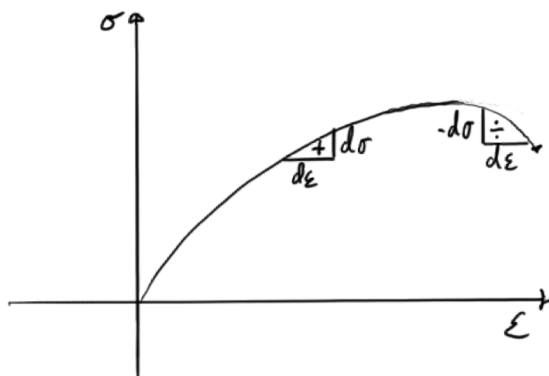

Figure 3.12 Non-negative work for stable materials

3.7 Post-crack behaviour: Flow rule and hardening rule

In this subchapter, we will briefly explain what we understand about the post-crack behaviour of concrete. Due to limitations in ANSYS we have not ventured deeply into this subject.

The William-Warnke model only specifies the stress needed to reach yielding in the material. Up until this point the material is assumed to behave elastically, even beyond the proportionality limit.

To describe the behaviour after yielding it is necessary to establish a flow rule and a hardening rule.

3.7.1 Flow rule

The strain rate in any material can be described as the sum of plastic strain rate and the elastic strain rate.

$$d\varepsilon = d\varepsilon_p + d\varepsilon_E$$

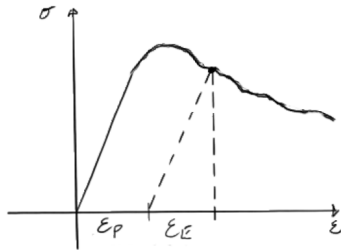Below is a figure where the strains are noted

Figure 3.13 Sketch of plastic and elastic strain

Through algebraic manipulations the following relationship can be found

$$d\varepsilon_p = \lambda \cdot \frac{dQ}{d\sigma_{ij}}$$

where,
λ is a hardening parameter
Q is the flow potential
σ_{ij} are the components of the stress tensor

In cases where Q is the yield function we have a so-called associative flow rule. The term $\frac{dQ}{d\sigma_{ij}}$ represents a normal to the yield surface in this case and is then related to the principle of normality.

Otherwise the flow rule will be non-associative.

In complicated yield criterions such as the William-Warnke model, a simpler Q can be used for approximation of the flow rule.

3.7.2 Hardening rule

After plasticity has been reached, further straining of the material will change the yield surface. This can happen either by isotropic hardening or softening, kinematic hardening or perfect elastic-plastic behaviour.
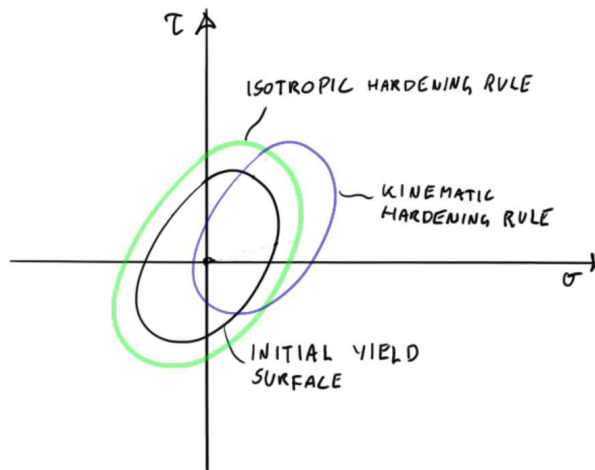

Figure 3.14   Sketch showing possible changes in the yield surface

We are interested in modelling the descending portion of the stress/strain diagram for concrete:
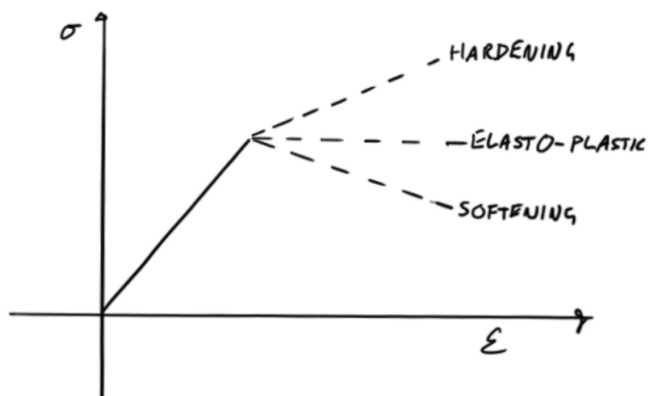

Figure 3.15 Stress-strain diagram showing different hardening rules

As it turns out, the concrete material model in ANSYS and the element type SOLID65 are restrictive in controlling the hardening behaviour. In the next sub chapters, we touch onto this issue.

3.8 ANSYS element types used in the tests

The information in this sub chapter is mainly drawn from the documentation for ANSYS [17]

3.8.1 SOLID65

The element consists of 8 nodes and $2x2x2$ gaussian integration points. Each node has $2 \cdot 3 = 6$ degrees of freedom. The element can simulate cracking or crushing behaviour if the stresses reaches yield strength. The corresponding stiffness matrix elements is then reduced to a small value. Stresses will be redirected to nearby elements and by this simulate crack growth. The simulated cracks can be displayed as a plot in ANSYS.

It is possible to add reinforcement to SOLID65 through its "real constants." The element will then look like this:
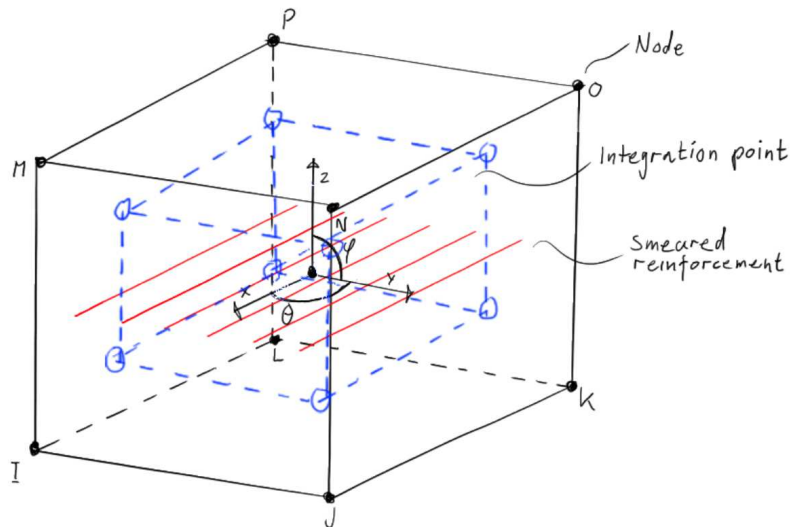

Figure 3.16 SOLID65 element with "Smeared reinforcement" indicated

This can be used to simulate normal reinforcement in the concrete and, to some extent, fibre-reinforcement. The "real constants" allow specifying 3 different reinforcing elements with individual material models, volume fractions and orientations in two directions (θ, φ). The reinforcement is "smeared" across the SOLID65 element with a thickness corresponding to the specified volume fractions. The reinforcement is activated once the SOLID65 element itself cracks or crushes. Cracks are signified by circles and can occur in the three principal directions. They are colored red, green and blue in that order. If crushing of the concrete is simulated, this is marked with a red octahedron.

3.8.2 SOLID185
This element type is similar to SOLID65 but is not capable of simulating cracking. Thus, the element type is less suited for use with concrete structures. It is, however, convenient to use for modelling steel plates at supports and concentrated loads.

3.8.3 LINK180
This is a 3D line element with 2 nodes, each with 3 degrees of freedom. The element type will commonly be used to model normal reinforcement. It is necessary to specify sectional area through "Sections" -> "Link" in ANSYS. This allows specifying the sectional area of the reinforcement.

3.9 ANSYS material models used in the tests
The information in this sub chapter is mainly drawn from the documentation for ANSYS [17]

3.9.1 Isotropic linear elasticity
This is one of the simplest material models in ANSYS and only needs the E-modulus and the Poisson's ratio to be specified. This material model is used for all element types to describe their linear elastic behaviour.

3.9.2 Von Mises bilinear plasticity with isotropic hardening

This model is used for reinforcement in the concrete. Up until yielding the steel follow an isotropic linear elastic model. At yielding stress, a tangent modulus is specified. The tangent modulus describes the slope of the stress-strain curve after yielding of the material. This slope must be positive which forces strain hardening behaviour of the material.
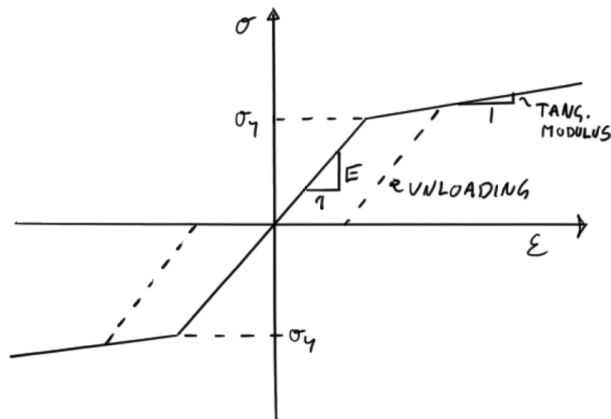

Figure 3.17 Bilinear plasticity with isotropic hardening

3.9.3 Concrete

ANSYS has a ready concrete model. This model is based on the Williams Warnke yield criterion with a "cut-off" in pure tension. The cut tension part is modelled with what appears to be the Rankine maximum principal stress theory. For triaxial and biaxial compression, the failure surface uses the William-Warnke criterion. For biaxial compression this is modified a little so that the failure surface is adjusted depending of the magnitude of the tensile stress. In biaxial tension the yield surface is drawn as straight lines between max compressive strength and max tensile strength. This is akin to the maximum shear stress theory or the Tresca criterion. In biaxial stress space, the yield surface looks like this:
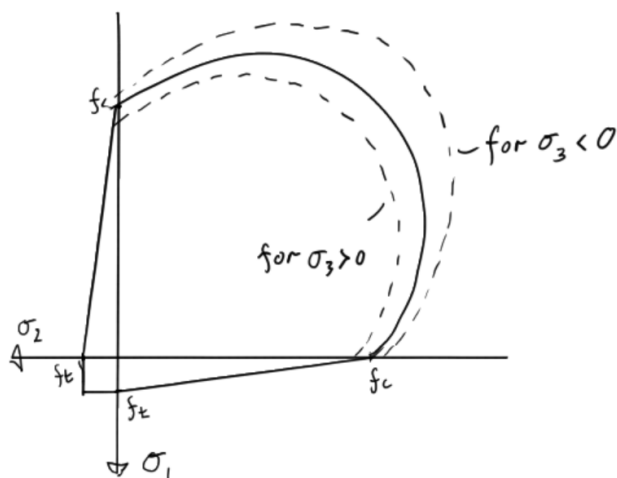

Figure 3.18 Biaxial yield envelope for the concrete material model in ANSYS

For the concrete model to work, only f_c and f_t needs to be specified. Default values are then assumed for biaxial strength (f_b) and uniaxial strengths ($f_{c,h}/f_{t,h}$) imposed on a hydrostatic pressure. The values are extracted from the original article on the model (William, Warnke [15]). The values are shown below:

$$f_b = 1.2 \cdot f_c$$
$$f_{t,h} = 1.45 \cdot f_c$$
$$f_{c,h} = 1.725 \cdot f_c$$

The default value for hydrostatic pressure is unknown, but we expect ANSYS to either recalculate it with every substep or use a maximum of $\sqrt{3} \cdot f_c$.

For the case of a stronger and more brittle concrete like UHPFRC, all these values should be considered. From chapter 4.3, we know that UHPFRC with around 2% volume fraction of randomly oriented steel fibre can be expected to behave like concrete. The default values indicated above may then be a sufficiently close approximation. But, there is no way to be sure that the fibres are isotropically oriented and uniformly packed in the entire concrete structure. It is not possible to change the concrete material model in ANSYS so that the yield surface represents non-isotropic fibre efficiency.

In addition to the strength parameters, it is possible to specify a ratio for transferring shear stresses across closed or open cracks. In the documentation for ANSYS it is simply stated that the ratio is between 0 (a very smooth crack) and 1 (a very rough crack).

Several articles refer to work done by Kachlakev [17] who proposes the values for <u>open</u> cracks to be 0.2. Apparently, this setting is changed mainly to improve the chances of convergence on simulation solutions. We use the proposed value and set the value for <u>closed</u> cracks to 0.8.

A tensile stress relaxation ratio at cracking can also be set. The default value of 0.6 is used in all our tests.

Lastly, it is stated that the model <u>may</u> undergo plasticity, with the Drucker-Prager plasticity model being the most common.

3.9.4 Drucker-Prager plasticity
This model is described earlier in chapter 3.5.2, but a short recap is provided here.

The Drucker-Prager yield surface is defined with values for cohesion and internal friction angle. In addition, a flow rule can be established through the angle of dilatancy. The yield surface is constant which describes an elasto-plastic hardening behaviour.

Since the concrete material only predicts the yield stress, a combination with the Drucker-Prager model can simulate post-crack behaviour. In this case it will be an inaccurate model since it is not possible to define a strain hardening or -softening behaviour.

For this combination to work, the Drucker-Prager yield surface must lie within the yield surface of the concrete model. In this way the material will reach yielding through the concrete model and will use the flow- and hardening rule from Drucker-Prager to simulate post-crack behaviour. We are a little unsure exactly how this will work, but below is a sketch of our thoughts.
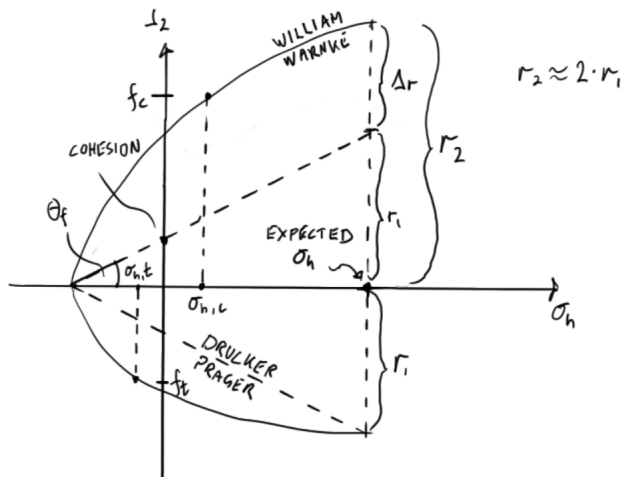

Figure 3.19 Drucker-Prager yield surface defined inside William-Warnke yield surface

4 Research question

The initial topic of this thesis was to find connections between composition, mechanical properties, structural behaviour and design rules for UHPFRC. This is a wide and general topic which gave us the opportunity to focus on what we thought would be interesting. We knew through previous courses that ANSYS had a material model valid for concrete.

From this we defined a more specific research question:

How can we analyse UHPFRC beams with the help of ANSYS?

To answer this question we also defined two operational questions:

How does the built-in concrete material model in ANSYS work?
How can the concrete material model in ANSYS simulate behaviour of UHPFRC beams?

4.1 Limitations

We limit the scope of the work by analysing two beams drawn from UHPFRC beam research done by Kamal et. al. [18]. The goal of that research was to study the shear behaviour of UHPFRC beams with and without shear reinforcement and with differing kinds of fibres. This is discussed more in detail in chapter 5, "Test Cases."

For the work done in ANSYS, we only use the material models found directly in the Graphical User Interface of the software.

5 Test Cases

The test cases described below originates from the work done by Kamal et. al in 2013 [18]. They have tested two sets of beams. The first set were beams reinforced with only flexural reinforcement. The second set also had shear reinforcement and compression reinforcement at the top. The goal was to examine the behaviour of beams under flexural load. And to study the effect of the fibre reinforcement with and without shear reinforcement and compression reinforcement. We have chosen two of the beams as test cases for our work in ANSYS.
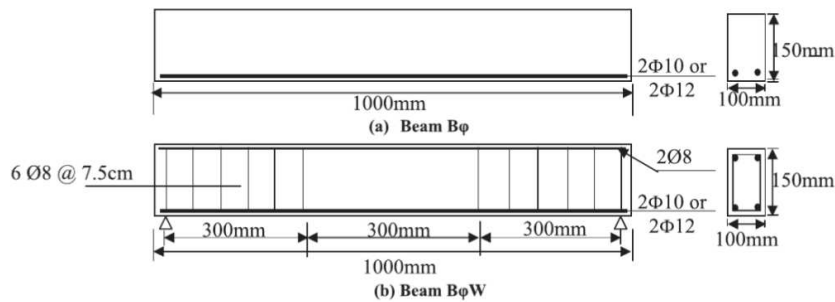

Figure 5.1 Sketch of geometry and reinforcement information of the two test beams

Figure 5.1 shows the geometry and reinforcement information of the two beams.

The one at the top is named B10S, due to flexural reinforcement of 2ϕ10mm.

The one at the bottom is named B10WS. It has flexural reinforcement of 2ϕ10mm, stirrups of 6ϕ8mm with 75mm spacing and compressive reinforcement of 2ϕ8mm.

Table 2	Compressive strength of the different concrete mixes.		
Mix No	Types of fibers	Compressive strength (Mpa)		
		3 days	7 days	28 day
1	–	43.0	67.4	127.0
2	Steel fibers	64.3	88.0	135.0
3	Polypropylene fibers	49.0	77.6	130.0

Figure 5.2 Compressive strength of the different concrete mixes

Figure 5.2 shows a table of the different concrete mixes and their characteristic compressive strength at 3, 7 and 28 day's tests. We only consider the beams with mix no. 2 which has steel fibre-reinforcement.

Table 1	Mix proportions.						
Mix No	Materials Required For One Cubic Meter (Kg)						
	Cement	Silica fume	Sand	Water	Superplasticizer	Steel fibers	Polypropylene fibers
1	874	97	1012	291	4.9	–	–
2						40	–
3						–	1

Figure 5.3 Mix proportions of three recipes

Figure 5.3 shows the mix-proportions of the three different UHPC recipes. They are all the same except addition of steel fibres to mix no. 2 and polypropylene fibres to mix no. 3.
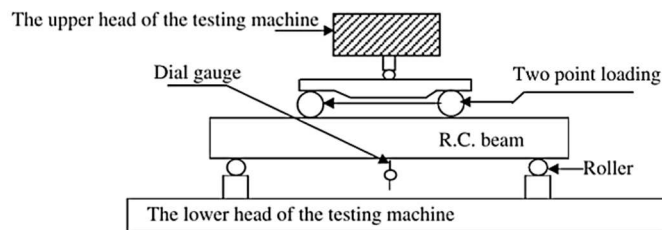

Figure 5.4 Testing machine and test set-up of the tested beams

Figure 5.4 shows the testing machine and test set-up of the tested beams.
This is a four-point bending test where the total force applied to the beam is applied by two concentrated loads. It seems that these concentrated loads are located on top of the stirrups closest to the center of the beam. That is 300mm from the roller supports which is located with an offset of 50mm from the beam-ends. The drawing shows that the beams have 6ϕ8 stirrups with spacing 75mm. This gives 375mm and not 300mm. In our test setup we used 5ϕ8 instead, which gives 300mm.

Figure 5.5 Crack pattern of beam B10S at failure

Figure 5.5 shows the crack pattern and failure mode of beam B10S. They report diagonal tension as failure mode. This can be seen at the left-hand side of the beam.
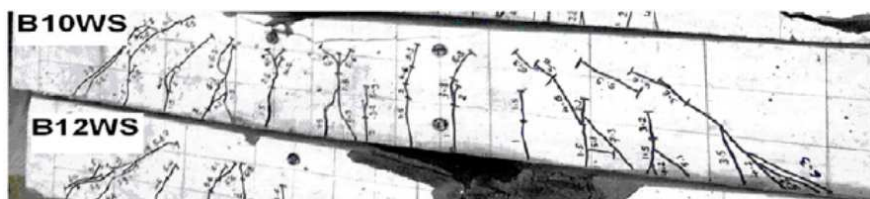

Figure 5.6 Crack pattern of beam B10WS at failure

Figure 5.6 shows the crack pattern and failure mode of beam B10WS. They report flexural failure. From the image above, we can see crushed concrete beneath the concentrated load on the left.

Table 4   Experimental test results for beam specimens.

Code Number	Initial cracking load (kN)	Ultimate load (kN)	Deflection (mm)		Ductility index	No. of cracks at failure	Failure mode
			Δy	Δu			
B10	20.0	36.4	–	–	–	10	Diagonal tension
B12	28.8	44.2	–	–	–	14	Diagonal tension
B10W	11.0	69.1	6.48	7.88	1.22	22	Flexural
B12W	20.0	98.5	5.68	6.79	1.19	21	Flexural
B10P	10.0	41.9	–	–	–	11	Diagonal tension
B12P	25.0	54.0	–	–	–	10	Diagonal tension
B10WP	11.0	71.4	12.13	15.98	1.32	23	Flexural
B12WP	18.0	105.8	5.00	7.56	1.51	28	Flexural
B10S	12.9	53.8	–	–	–	11	Diagonal tension
B12S	15.0	60.4	–	–	–	14	Diagonal tension
B10WS	10.0	78.3	9.23	14.23	1.54	16	Flexural
B12WS	27.0	103.8	6.25	10.88	1.74	21	Flexural

Figure 5.7 Experimental test results for all the beam specimens

Figure 5.7 shows the experimental test results for all the beam specimens. Outlined in red is beams considered in this thesis.
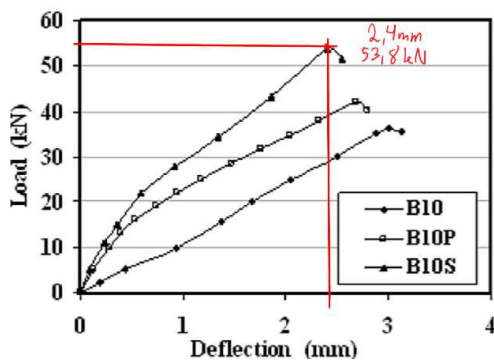

Figure 5.8 Load/Deflection diagram of B10S

Figure 5.8 shows the Load/Deflection diagram for B10S. Deflection of this beam is not reported. With help of this Load/Deflection diagram we set the deflection to be 2.4mm at reported failure load 53.8kN.
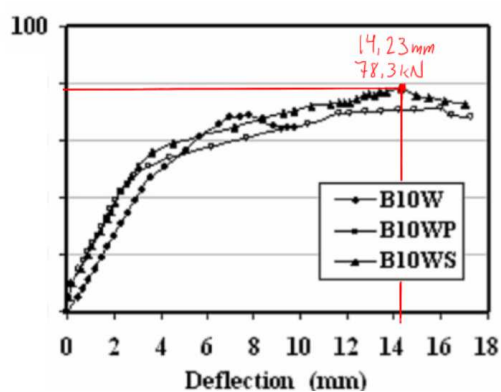

Figure 5.9 Load/Deflection diagram of B10WS

Figure 5.9 shows the Load/Deflection diagram for B10WS. Red values are from figure 5.7 which shows 14.23mm deflection at failure load 78.3kN for this beam.

6 Method

Our work has been an iterative process where we have changed between acquiring knowledge and modelling in ANSYS. The theory and the test results must be understood as the sum of all this work. In a similar manner the workflow in ANSYS, presented later in this chapter, is based on the results from the preliminary testing. These tests are presented at the start of chapter 7.

6.1 Strategy

6.1.1 Literature review

The literature review runs parallel to the work in ANSYS throughout the entire project period. Theory found this way is presented in chapter 3.

Test cases for our work in ANSYS are also found and is presented in chapter 5.

6.1.2 Hypotheses testing on test cases

Conjectures on how to model and predict behaviour of UHPFRC beams are drawn from literature. A hypothesis is made on this background. The test cases are simulated in ANSYS and analysed. The results from the simulations are compared to the actual test results and discussed. Depending on the outcome of the test, either the theory, the hypothesis or the test is refined. This method is known as the hypothetico-deductive method and is widely employed in engineering and natural science applications. Below is a flow chart describing the phases of the method.
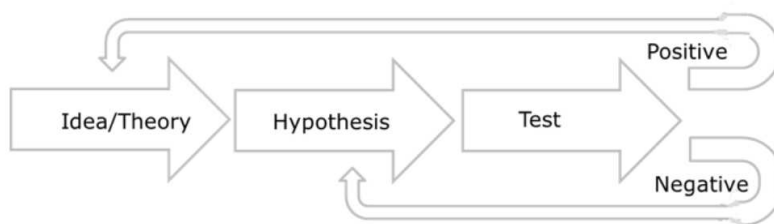

Figure 6.1 Flow chart of the hypothetico-deductive method

6.1.3 Learning ANSYS

To simulate the test cases, it is necessary to acquire knowledge on how to use ANSYS. Some basic knowledge in ANSYS is gained through previous courses, but we must continuously improve our workflow. The culmination of what we have learned about working in ANSYS is outlined below.

6.2 Overview of workflow in ANSYS

6.2.1 Structure modelling, boundary conditions and discretization into FEM-mesh

The element type SOLID65 is used to model the beams. The mesh is always quite coarse, and the element size is a common multiple of the beam dimensions. First and foremost, this is to reduce calculation time which can be many hours if the mesh is very fine. Also, since we are using the student version of the program, there are a limited number of nodes and elements we can model.

It is possible to model half of the beam and apply a symmetry boundary condition along its central longitudinal direction. We decided against doing this in the transverse direction since this will make the beams statically indeterminate.

Fibre reinforcement can be added to SOLID65 via "Real Constants." The default input parameters define material model, volume fraction and orientation in two directions for the reinforcement. The intricate behaviour of the fibres must then mainly be determined in the material model of the fibres.

For supports and concentrated loads a small steel plate is modelled using SOLID185 elements. The mesh of this plate must match the mesh of the concrete structure exactly. This is needed so that the nodes later can be merged to facilitate transfer of loads throughout the entire structure.

The element LINK180 is used to model reinforcement. A line is drawn exactly through the nodes and then meshed with the same element size as the concrete mesh. This is done to save time. As for the steel plates, this allows merging of the nodes so that loads can be transferred between rebar and concrete. Through its "Real Constants" it's possible to define the sectional area of the rebar and decide if it can take compressive and/or tensile forces.

To save time and reduce complexity of the model, we allow the reinforcement to be placed at the nearest node in the concrete mesh. The error in the position of the rebar is usually in the range of 5-10mm depending on mesh element size and diameter of the rebar. This potential offset in rebar location will have negligible impact on the results.

The loads are applied as stresses on top of the steel plates. This will reduce stress concentrations even more. Support conditions are applied as a zero-displacement control at the central nodes on the support plates. This allows the structure to rotate freely at the supports and no extra stresses are induced.

6.2.2 Material models

All mesh elements must be associated with a material model. This determines the elements behaviour when exposed to stresses and strains. In this study we have used the models found through the graphical user interface of ANSYS.

The first material model used to model UHPC is the built-in CONCR model in ANSYS. As mentioned in the theory chapter this model is based on the WW-model. It has a cutoff in tension and uses the simpler Rankine model instead. The theory behind these models are discussed in the theory chapter of this thesis, see chapter 3.9.3.

Later a Drucker-Prager plasticity model was also added to the UHPC elements. This is done to simulate plastic deformation without explicitly defining the steel fibres. With the built-in model, only the flow rule is defined via the dilatancy angle. This means that an elasto-plastic hardening rule is applied, which is a simplification of the real behaviour. This is discussed in the theory chapter 3.5.2. For this to work, this model must lie within the William-Warnke failure envelope. For simplicity, the parameters are calculated with $\frac{f_c}{2}$ (see chapter 3.9.4)

For the steel plates a simple linear elastic isotropic material model is used. The steel plates are only there to reduce the artificially high stress concentrations near corners and concentrated loads.

For the reinforcement, an inelastic bilinear isotropic model is used. The inelastic part is defined by the yield strength of the steel. This is to prevent the rebar from taking up too much stress.

If fibres are added to the SOLID65 elements, a simple linear elastic isotropic material model is used. To simulate the behaviour of the fibres, different elastic moduli and Poisson's ratios have been applied. The main reason for using fibres in this way is to bridge cracks and simulate plastic behaviour.

Some of the difficulties of modelling fibres this way is briefly touched into in the theory chapter with a more thorough discourse in the discussion chapter.

6.2.3 Simulation

After the structure, materials and boundary conditions are modelled, the simulation can be run.

For simplicity, only the static solution is sought and a relatively small amount of solution substeps are used. The solver is set to run a "small displacement static analysis." The solution of every substep is saved for later review.

Due to the highly non-linear nature of the model, ANSYS is allowed to run a maximum of 200 iterations on each substep to increase the chance of converging on a solution.

The solver is usually set to converge with respect to displacement only. This makes it easier to obtain a solution. After each simulation a reference value for the convergence criterion is saved. The next simulation will use this value from the start. If a simulation stops because of excessive displacement, care must be taken to reset this reference value to zero. Otherwise, the next simulation will use an inflated convergence criterion value and there is a risk that this will produce wrong results.

6.3 Hypotheses Test Setup

For consistency we lock as many parameters as possible. Below are tables containing the parameters that is common for all the tests. The concrete models and other unique parameters are presented before each hypothesis test.

The concrete E-modulus and tensile strength are calculated with (3.1) and (3.2), respectively.

Setup	Structure	Element type	Material model	Material parameters	
Common	Bottom reinf. Top reinf.	LINK180	Linear isotropic	E-modulus (MPa)	200000
				Poisson's ratio	0.3
			Bilinear isotropic	Yield stress (MPa)	550
				Tangent modulus (MPa)	50
			Real constant (Bottom)	Sectional area (mm2)	78.54
			Real constant (Top)	Sectional area (mm2)	50.27
	Shear reinf.	Link180	Linear isotropic	E-modulus (MPa)	200000
				Poisson's ratio	0.3
			Bilinear isotropic	Yield stress (MPa)	350
				Tangent modulus (MPa)	35
			Real constant	Sectional area (mm2)	50.27
	Steel plates	SOLID185	Linear isotropic	E-modulus (MPa)	200000
				Poisson's ratio	0.3

Figure 6.2 Common material parameters in ANSYS

ANSYS Solver	
Small displacement static	-
Convergence criterion	Displacement
Convergence norm	Infinite
Tolerance	0.001
No. Substeps	50
Max. Iterations pr substep	200

Figure 6.3 Common solver setup in ANSYS

6.4 Quick overview of the work in this project

Phase 0:　　Initial learning of ANSYS
　　　　　　Preliminary literature study
　　　　　　Initial theoretical framework and hypothesis
Phase 1:　　Testing hypothesis 1
Phase 2:　　Theoretical work, learning ANSYS, literature study and refining hypothesis
　　　　　　Testing hypothesis 2
Phase 3:　　Theoretical work, learning ANSYS, literature study and refining hypothesis
　　　　　　Testing hypothesis 3
Phase 5:　　Report findings

The hypotheses and the results are presented in the next chapter.

7 Results

This chapter contains the results from our tests in ANSYS. The main part of the chapter is the testing of different hypotheses. These tests are done as described in the method chapter. There are three hypotheses to be tested. Each test has a test setup, the deriving of the hypothesis, test results and a brief examination of the results. This examination is important because the next hypothesis builds on the results from the previous tests. After the hypothesis tests a short summary is included followed by four more tests with increased moment.

The chapter starts with a description of the results from the preliminary testing.

7.1 Preliminary testing in ANSYS

Several attempts were made to figure out a decent setup to reliably get ANSYS to produce results. The problem, in the beginning, was getting ANSYS to find solution convergence to the simulations.
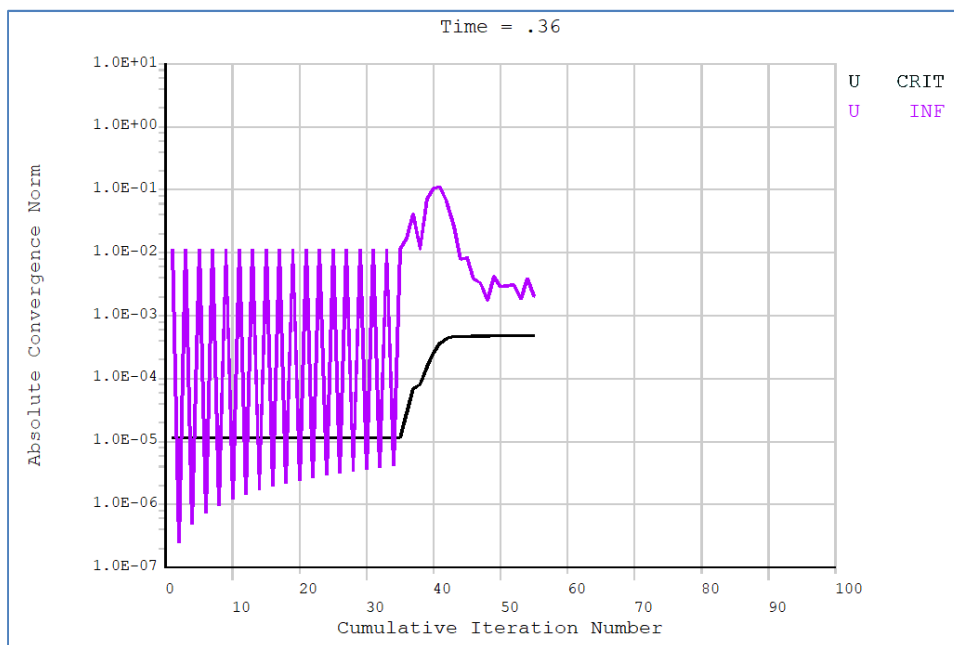
Figure 7.1 Typical simulation from the earlier tests

The figure above shows a typical simulation of the tests earlier in the project period. Any time the U,inf value goes below the U,crit we have convergence in the solution for the given substep (represented by "time" in the picture). After a reasonably stable initial period, there is a sudden change in the U,inf curve. This must be where the SOLID65 elements starts cracking which will dramatically change the stiffness matrices.

By default, the solver is set to seek convergence towards force equilibrium. By changing this to a displacement equilibrium criterion (as shown in the figure above), we found that the simulations converged easier.

We believed that increasing the amount of substeps would help solution convergence. Increasing substeps for the "Static" analysis type in ANSYS will reduce the amount of force added in each

28

substep. However, this did not help much in finding a solution and only added to the time it takes for a simulation to run.

We tried to use other solvers in ANSYS. The "large displacement static" helped a bit, but we got a warning that when used together with SOLID65 the results may be inaccurate. Also, it makes little sense to include geometrical nonlinearity in the simulation of the beams as failure should be reached well before 2nd order effects from deformation comes into play.

In addition, we tried to increase the convergence tolerance. This was eventually found to be unnecessary because the difference between the calculated values and the convergence criteria were usually too large.

Later, we discovered that a better method was to increase the amount of iterations ANSYS is allowed to run for each substep. The default "Prog Chosen" amount of iterations seems to be 20 (this can be seen in the "unstable" part of figure 7.1. This stops the simulation before convergence can be found. Setting the number of iterations to a higher amount increases the chance of finding converged solutions vastly. Furthermore, it allows us to use "small displacement static" solver and the default 0.1% convergence tolerance. All this at a cost of increased computation time.

The results of this work are used to revise the workflow in ANSYS as presented in chapter 6, "Method".

7.2 Structural model setup for hypotheses testing

The hypotheses are tested with the help of the two beams from chapter 5, "Test Cases". The original report is a little unclear on the placement of reinforcement and concentrated loads. It is stated that they use 6 stirrups at 75mm spacing over a distance of 300mm. The distance means that there is only space for 5 stirrups. Below is the model used in ANSYS for the tests:
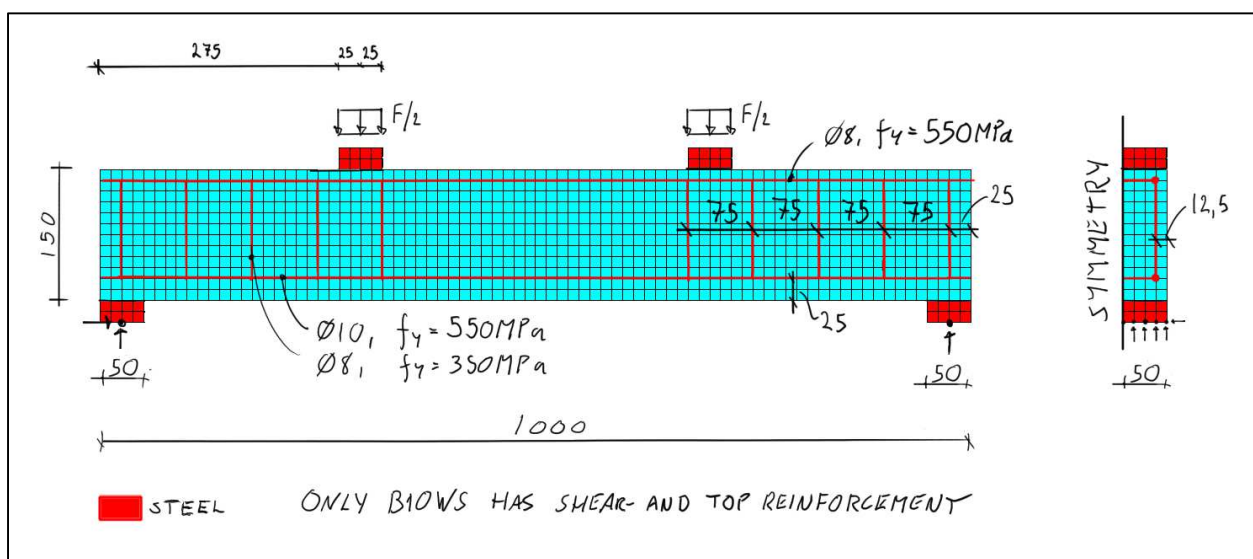
Figure 7.2 General geometry of the model with load and support conditions

UNIVERSITETET I AGDER

7.2 Hypothesis 1

To use the concrete material model in ANSYS, values for concrete E-modulus, Poisson's ratio, uniaxial tensile- and compressive strength are needed. The compressive strength is found in the original report on the test cases, but the other values need to be calculated.

The multiaxial behaviour of UHPFRC is ignored in this test. The reason being that the test cases are small beams and the multiaxial stresses are expected to have little impact. This could lead to inaccuracies, as the mix-design for the test cases only has 0.5% volume fraction of fibres. Chapter 3, the theory chapter, includes a discussion on this.

The calculated tensile stresses are assumed to include contribution from fibres. This also implies that the fibres are assumed to be oriented and packed so that they are equally effective at resisting tensile stresses at any point in the beam. This is because the assumed tensile strength is equal in all directions.

Hypothesis:
The concrete material model in ANSYS alone can predict the behaviour of the test cases.

7.2.1 Test Setup

Setup	Structure	Element type	Material model	Material parameters	
Common	Beam	SOLID65	Linear isotropic	E-modulus (MPa)	45241
				Poisson's ratio	0.2
			Concrete	Open crack ratio	0.2
				Closed crack ratio	0.8
				Uniaxial cracking (MPa)	7.55
				Uniaxial crushing (MPa)	135
				Tensile relax. ratio	0.6

Figure 7.3 Test Setup: Hypothesis 1

7.2.2 Results: Hypothesis 1 - Test 1 - B10S

HYPOTHESIS 1: TEST CASE B10S – CONCRETE MATERIAL MODEL
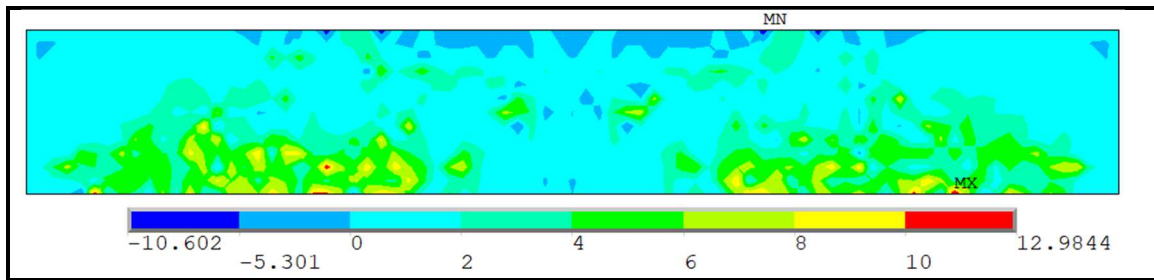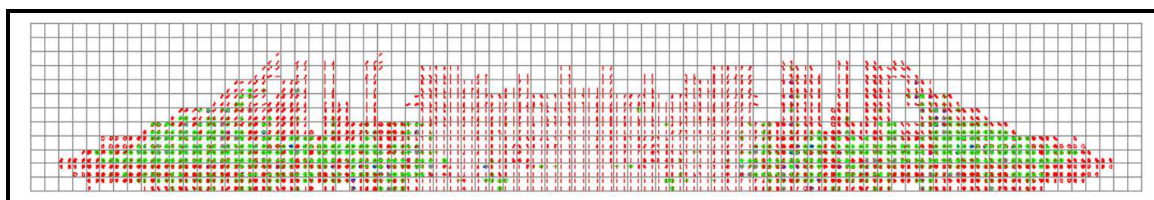

Primary Principal Stress (MPa)
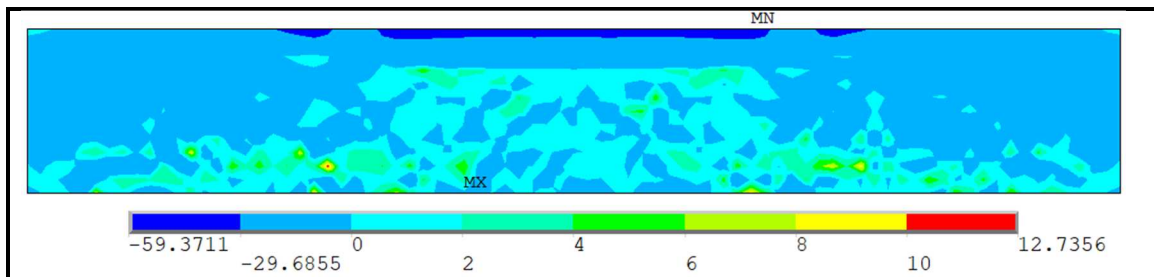
Normal Stress (MPa) in longitudinal direction
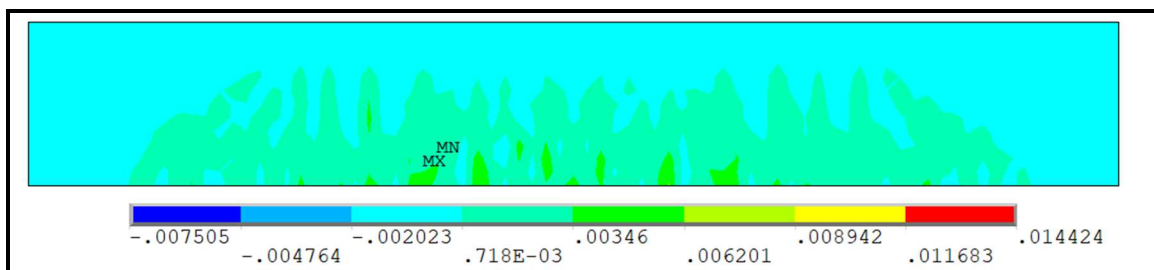
Elastic Strains in longitudinal direction
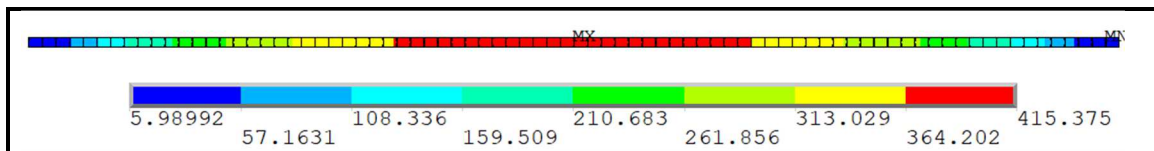
Tensile Stress in reinforcement

Simulated crack pattern

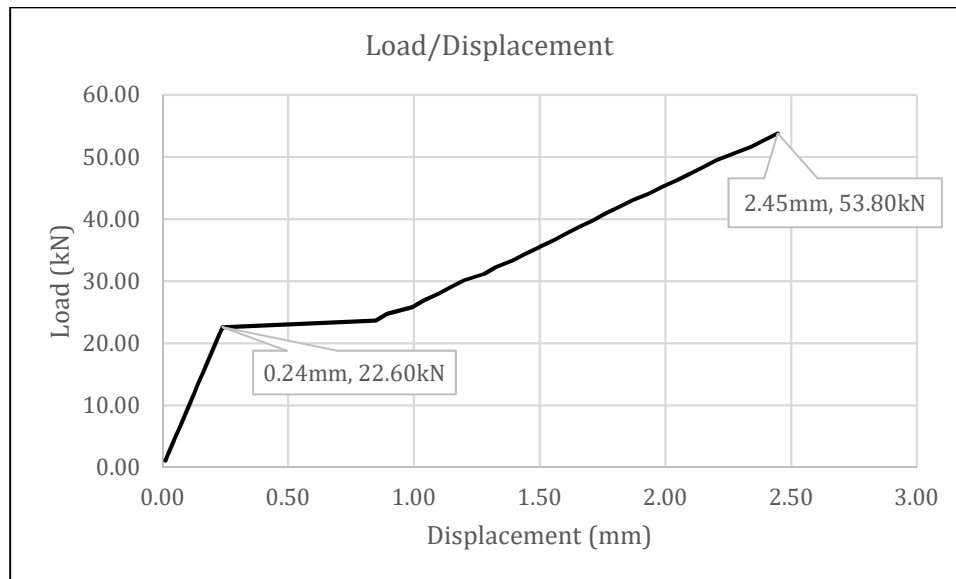*Figure 7.4 Plots: Hypothesis 1 - Test 1 - B10S*

Figure 7.5 Load/Displacement: Hypothesis 1 - Test 1

Results	Experimental	Simulated
Applied load (kN)	53.8	53.8
First crack load (kN)	12.9	22.6
Number of visible cracks	11	
Fracture type	Shear	
Deflection midspan (mm)	2.4	2.45

Figure 7.6 Results: Hypothesis 1 - Test 1

7.2.3 Observations: Hypothesis 1 - Test 1 (Case B10S)

- There are several areas with stresses above the tensile strength of the concrete. These are found both in the principal stress plot and in the normal stress plot. Note that these plots represent the stresses that are present for a given substep. Further loading would likely lead to cracking in the high stress areas and an immediate reduction of the stresses.
- In some areas along the top of the beam there are negative primary principal stresses. In these areas the elements are in a triaxial compression state, which activates the William-Warnke criterion. We remember that for all other stress states there is a tension "cut-off" in the model.
- It is interesting to observe the heights of the tensile and compressive zone in the normal stress plot. The concrete is still far from reaching compressive strength at 135MPa.
- The concrete material model does not undergo plasticity after yielding. The large strains are due to the concrete following the strains in the reinforcement.
- The simulation converged at a solution for the specified load (53.8kN).
- Note the large flat area immediately after cracking load in the Load/Displacement diagram

7.2.4 Results: Hypothesis 1 - Test 2 - B10WS
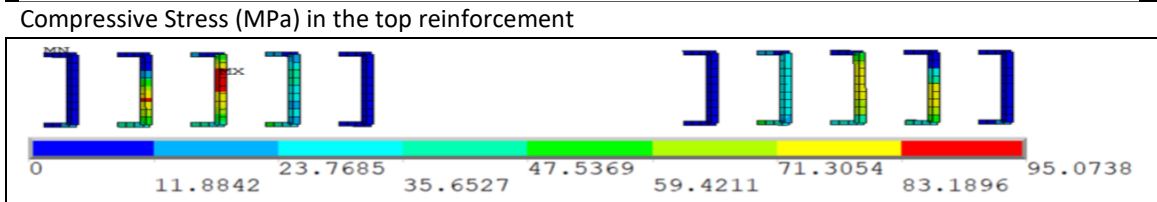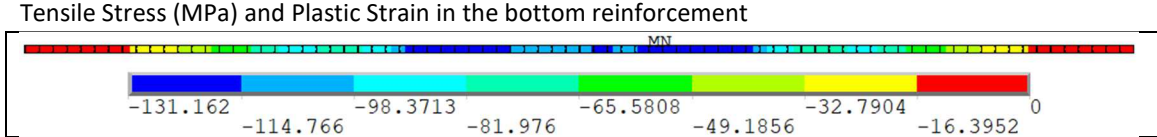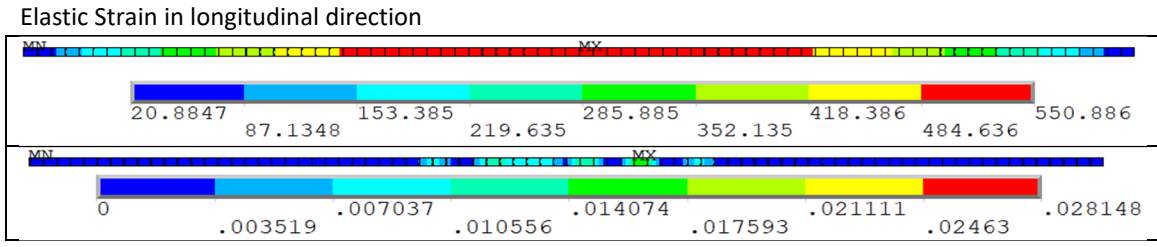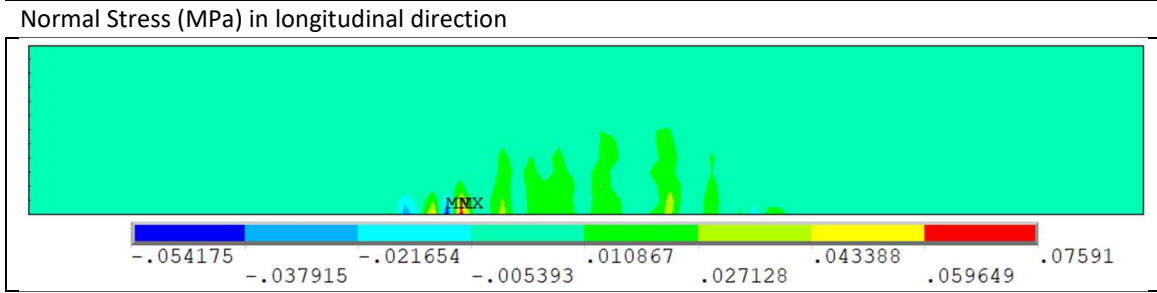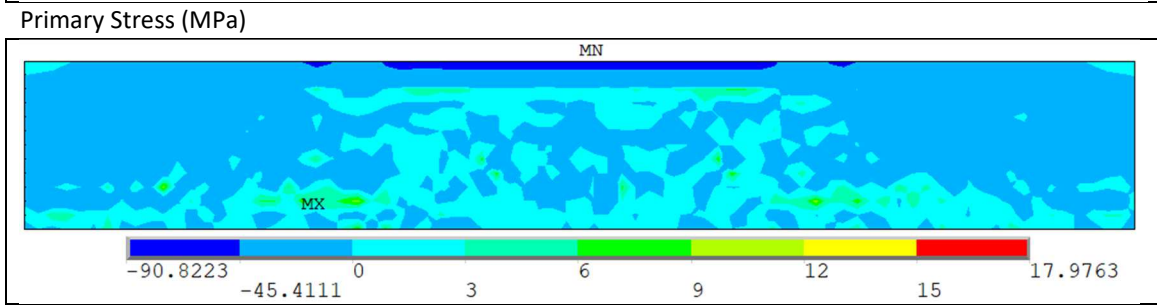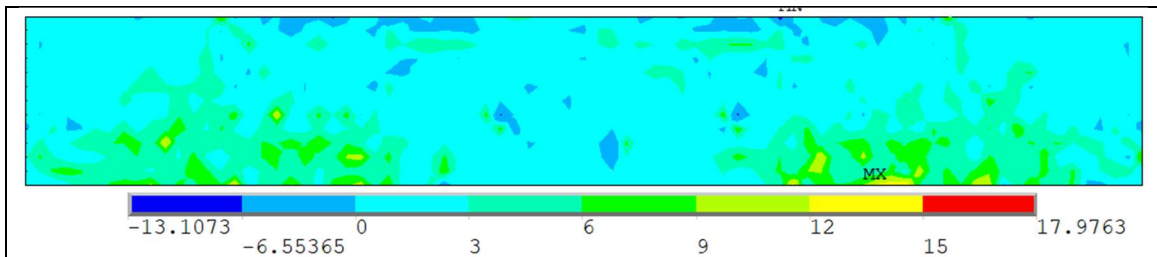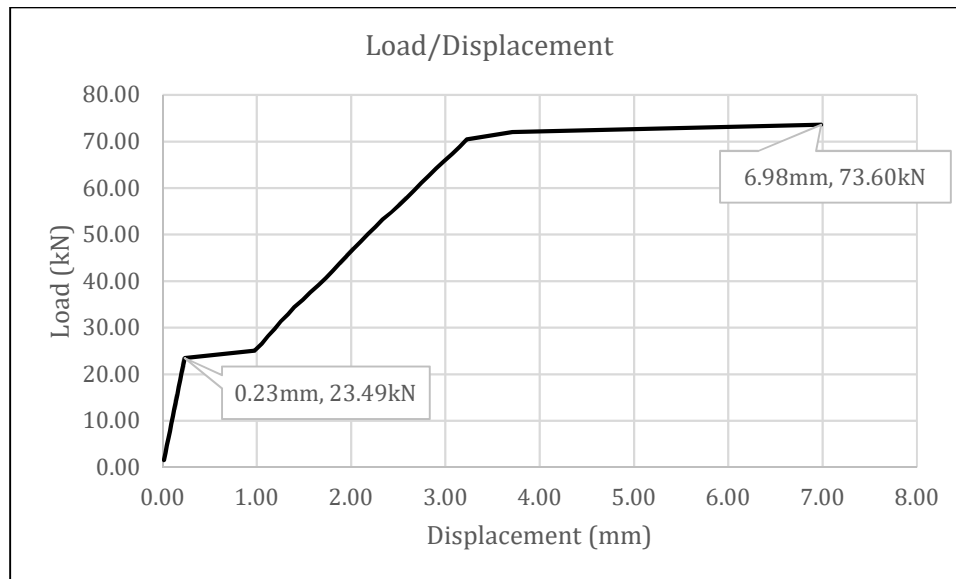
HYPOTHESIS 1: TEST CASE B10WS – CONCRETE MATERIAL MODEL

Primary Stress (MPa)

Normal Stress (MPa) in longitudinal direction

Elastic Strain in longitudinal direction

Tensile Stress (MPa) and Plastic Strain in the bottom reinforcement

Compressive Stress (MPa) in the top reinforcement

Tensile Stress (MPa) in the shear reinforcement

Simulated crack pattern
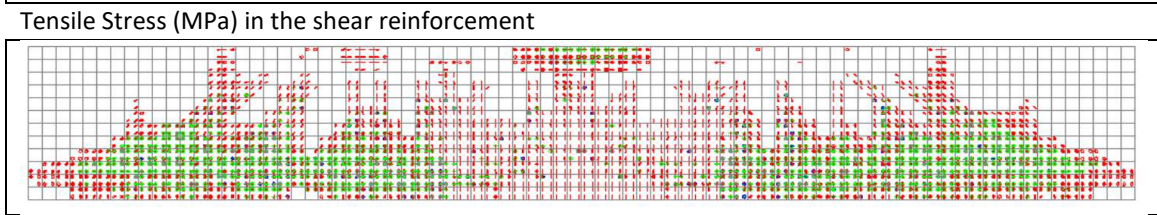
Figure 7.7 Plots: Hypothesis 1 - Test 2 – B10WS

Figure 7.8 Load/Displacement: Hypothesis 1 - Test 2

Results	Experimental	Simulated
Applied load (kN)	78.3	73.6
First crack load (kN)	10.0	23.49
Number of visible cracks	16	
Fracture type	Flexural	Flexural
Deflection midspan (mm)	14.23	6.98

Figure 7.9 Results: Hypothesis 1 - Test 2

7.2.5 Observations: Hypothesis 1 - Test 2 (Case B10WS)

- The solution stopped converging at 94% of ultimate load. The reason is most likely that the cracks have propagated all the way through the section at midspan. This indicates flexural fracture which is the same fracture type as the original test.
- The main reinforcement has yielded
- The deflection at this load is 49% of the reported value.
- The elastic tensile strains in the concrete corresponds to the plastic strains in the reinforcement.
- The stresses in the shear reinforcement follows the diagonal tension from the shear forces in the beam.
- There is a large flat area in the Load/Displacement diagram after the initial cracking load also for this test.

On the next page is the graph that shows what happens when the simulation fails to converge
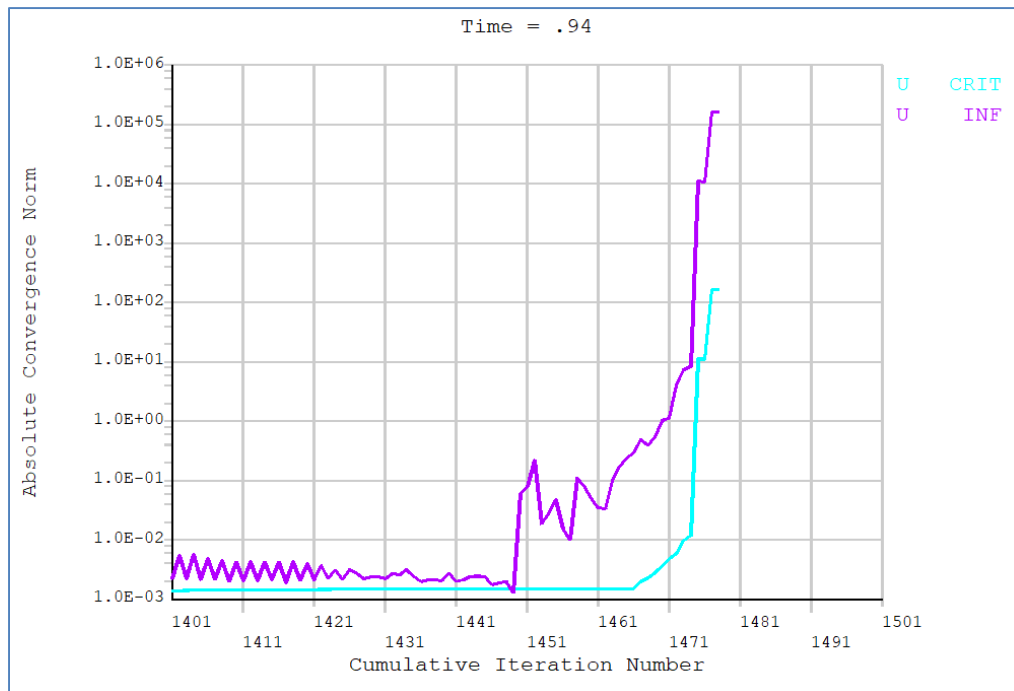
7.2.6 Solution non-convergence

Figure 7.10 Graph for a non-converged simulation

This is what should happen when the material loses stability. The displacement reaches towards infinite and a solution cannot be found.

7.2.7 Intermediate conclusion: Hypothesis 1

The Load/Displacement diagrams from the tests have a misplaced platform at cracking stress. This should lead to inaccuracies in the simulations.

7.3 Hypothesis 2

The force/displacement diagrams from the previous hypothesis test had a misplaced platform at cracking stress. This should cause some inaccuracies in the simulations. To rectify this, the fibres could be modeled in explicitly. This could potentially dampen the stiffness reduction in the cracked areas and allow a smoother flattening of the curve.

Due to the tensile strength is assumed to include the contribution from fibres, the fibre material model should not add any strength to the concrete. Instead only the improvement in ductility of the concrete is sought.

A simple model of the problem could be to just add the fibres as "smeared reinforcement" in the SOLID65 elements. The fibres are assumed to have isotropic orientation with a linear elastic model.

To see the effect of changing the fibre model, two simple models are used for the tests. The first one will have a linear elastic material model for the fibre where the E-modulus and Poisson's ratio is set the same as the concrete. The reason for this is that the stiffness of the fibres is vastly higher than that of the concrete and will likely add too much strength to the concrete.

For comparison, the second test will have half the E-modulus of the first test.

Hypothesis:
The concrete material model in ANSYS combined with a fibre model can predict the behaviour of the test cases.

7.3.1 Test setup

| Setup	Structure	Element type	Material model	Material parameters			Real Constants	
Common	Beam	SOLID65	Linear isotropic	E-modulus (MPa)	45241			
				Poisson's ratio	0.2			
			Concrete	Open crack ratio	0.2			
				Closed crack ratio	0.8			
				Uniaxial cracking (MPa)	7.55			
				Uniaxial crushing (MPa)	135		Real Constants	
				Tensile relax. ratio	0.6	Direction	Vfraction
Test 1 Test 3	Fibre 1	Real Constant to SOLID65	Linear isotropic	E-modulus (MPa)	45241	x = y = z	0.00167
				Poisson's ratio	0.2		
Test 2 Test 4	Fibre 2	Real Constant to SOLID65	Linear isotropic	E-modulus (MPa)	22621	x = y = z	0.00167
				Poisson's ratio	0.2		

Figure 7.11 Test setup: Hypothesis 2

7.3.2 Results: Hypothesis 2 - Test 1 - B10S (Fibre E = 45241)
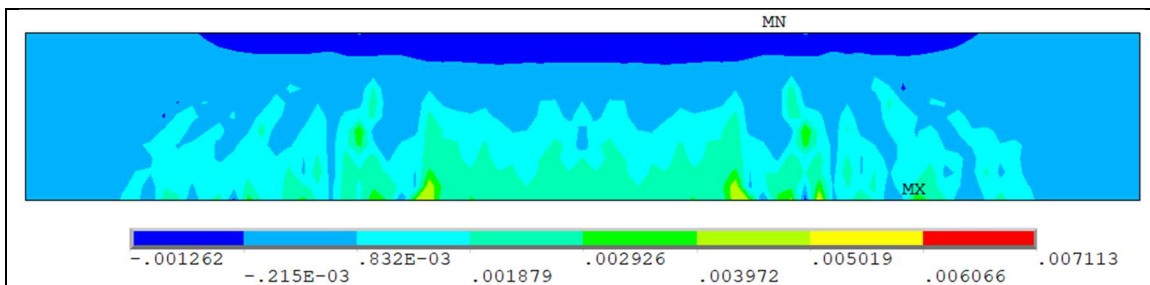
HYPOTHESIS 2: TEST CASE B10S – LINEAR ELASTIC FIBRE MODEL (E-MODULUS = 45241)
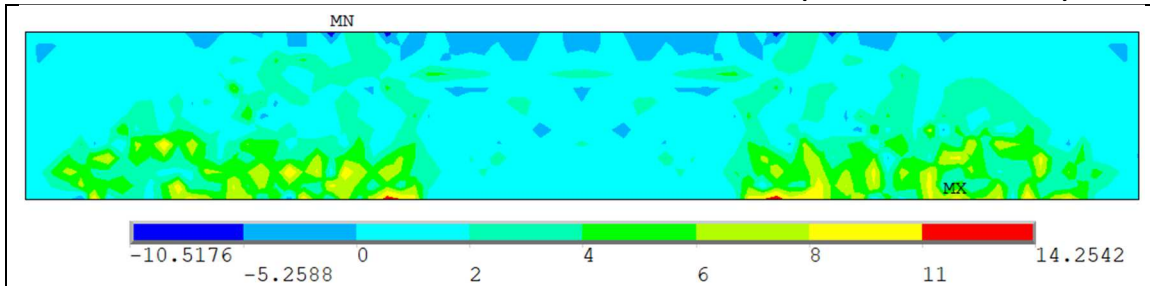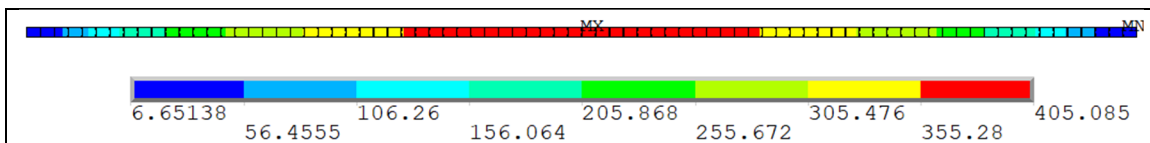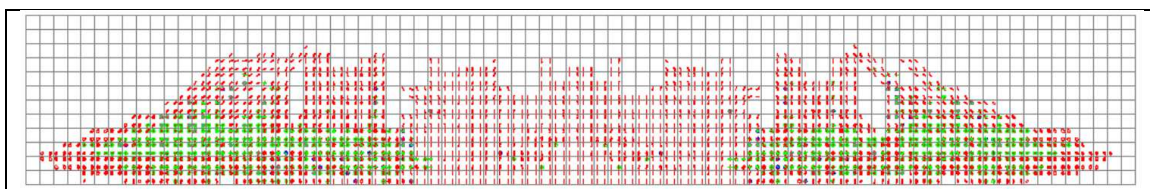

Primary Principal Stress (MPa)
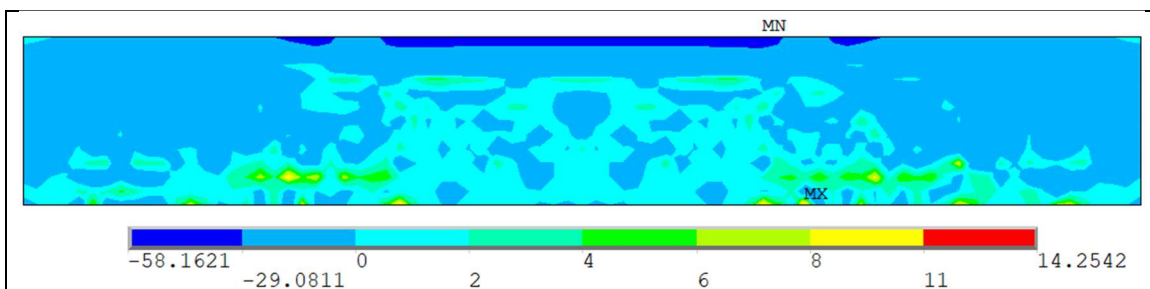
Normal Stress (MPa) in longitudinal direction

Elastic Strain in longitudinal direction

Tensile Stress in the reinforcement

Simulated crack pattern
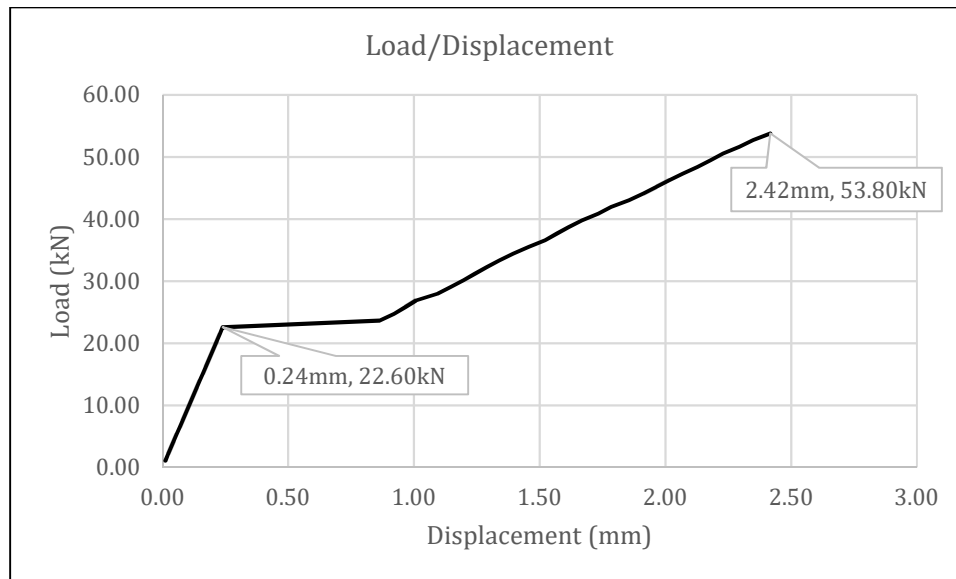
Figure 7.12 Plots: Hypothesis 2 - Test 1 – B10S

Figure 7.13 Load/Displacement: Hypothesis 2: Test 1

Results	Experimental	Simulated
Applied load (kN)	53.8	53.8
First crack load (kN)	12.9	22.6
Number of visible cracks	11	
Fracture type	Shear	
Deflection midspan (mm)	2.4	2.42

Figure 7.14 Results: Hypothesis 2 - Test 1

7.3.3 Observations: Hypothesis 2 - Test 1 (Case B10S)

- The results from this test is almost the same as test 1 from the first hypothesis.
- There are small differences in simulated deflection and the crack plot.
- There is a small increase in maximum tensile stress. This can indicate that the fibres have an influence on the results.
- The inclusion of smeared reinforcement has negligible effect on the flat area at cracking stress.

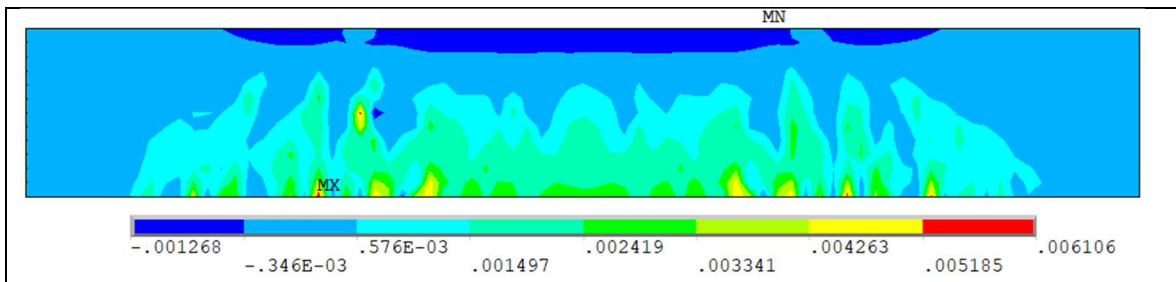## 7.3.4 Results: Hypothesis 2 - Test 2 - B10S (Fibre E = 22621)

HYPOTHESIS 2: CASE B10S – LINEAR ELASTIC FIBRE MODEL (E-MODULUS = 22621)
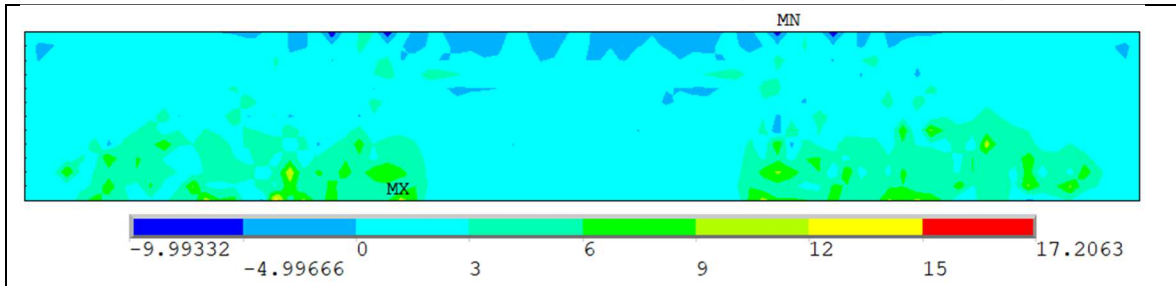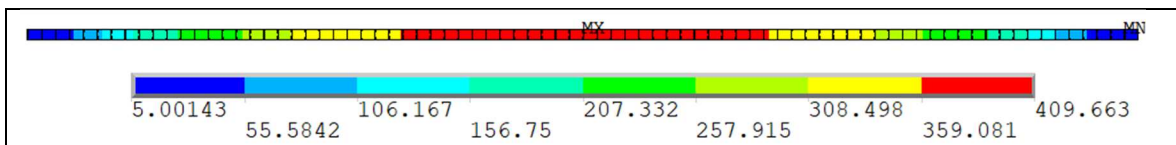
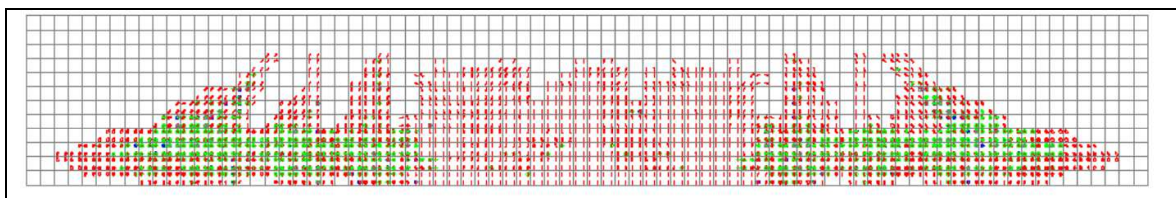

Primary Principal Stress (MPa)
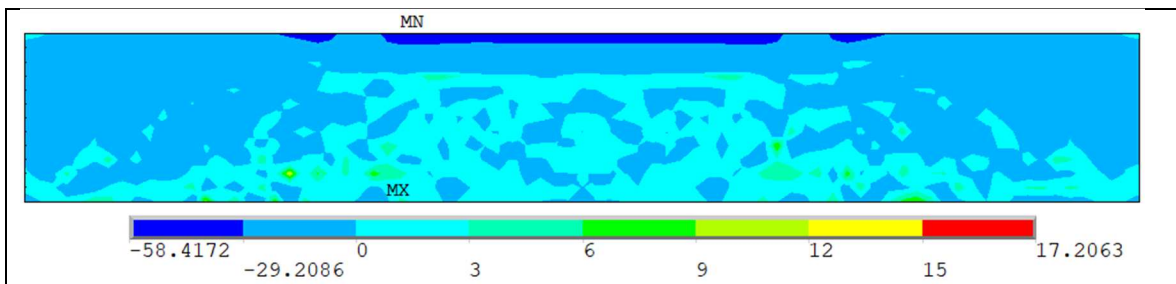
Normal Stress (MPa) in longitudinal direction

Elastic Strains in longitudinal direction

Tensile Stress (MPa) in reinforcement

Simulated crack pattern

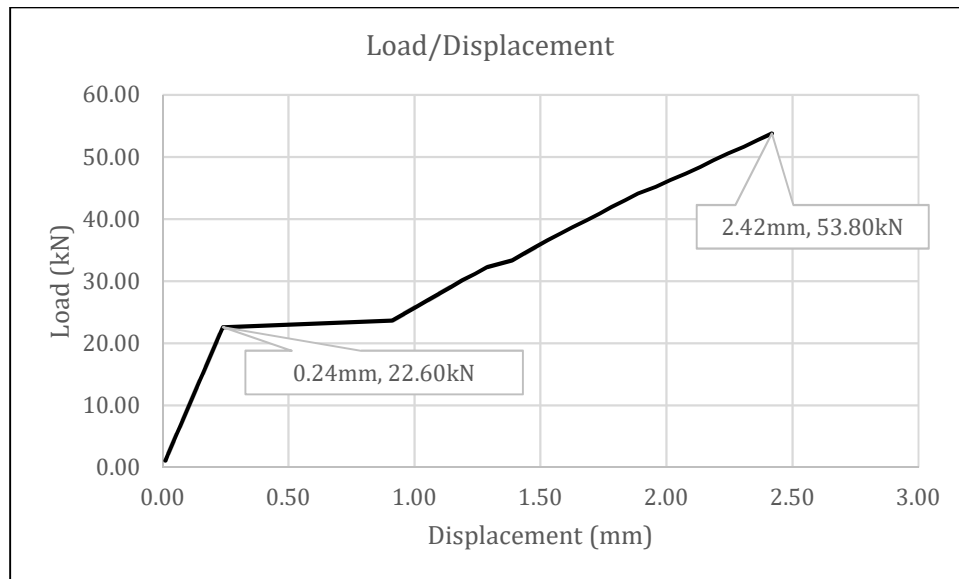*Figure 7.15 Plots: Hypothesis 2 - Test 2 – B10S*

Figure 7.16 Load/Displacement: Hypothesis 2 - Test 2 - B10S

Results	Experimental	Simulated
Applied load (kN)	53.8	53.8
First crack load (kN)	12.9	22.6
Number of visible cracks	11	
Fracture type	Shear	
Deflection midspan (mm)	2.4	2.42

Figure 7.17 Results: Hypothesis 2 - Test 2 - B10S

7.3.5 Observations: Hypothesis 2 - Test 2 (Case B10S)

- The perimeter of the cracked areas is a little more defined in this simulation compared with the first test.
- The maximum tensile stress in the concrete is now very high. It is now evident that these stress concentrations tend to occur near the bottom edge of the beam and the inner edge of the evolving stress area (see the "MX" in the principal stress plot)
- The maximum displacement is the same as for the previous test.
- The flat area is present in the Load/Displacement diagram.

7.3.6 Results: Hypothesis 2 - Test 3 - B10WS (Fibre E = 45241)

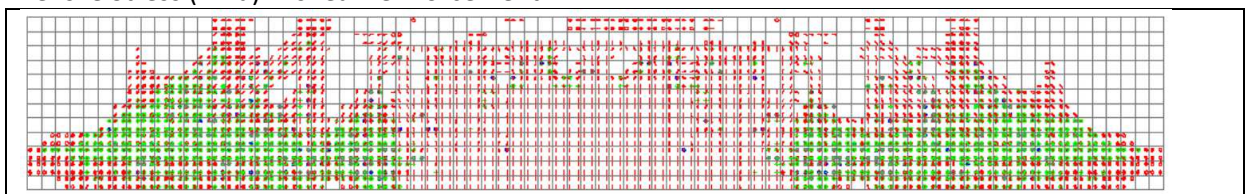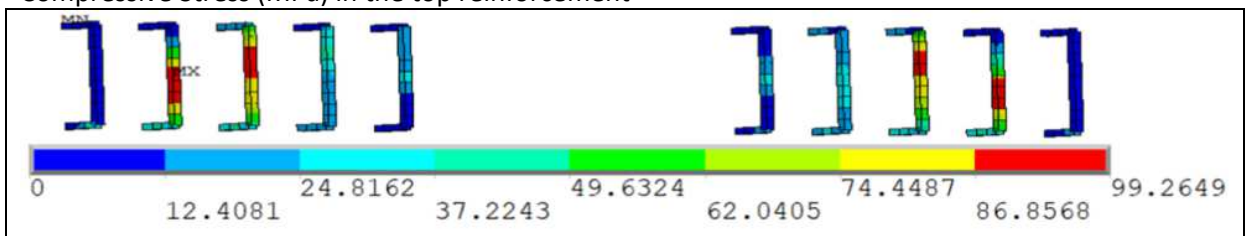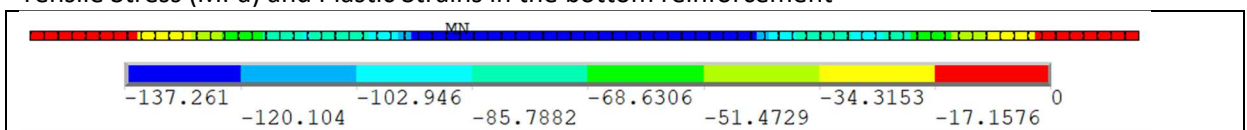**HYPOTHESIS 2: CASE B10WS – LINEAR ELASTIC FIBRE MODEL (E = 45241)**

Primary Principal Stress (MPa)

Normal Stress (MPa) in longitudinal direction

Elastic Strains in longitudinal direction

Tensile Stress (MPa) and Plastic Strains in the bottom reinforcement

Compressive Stress (MPa) in the top reinforcement
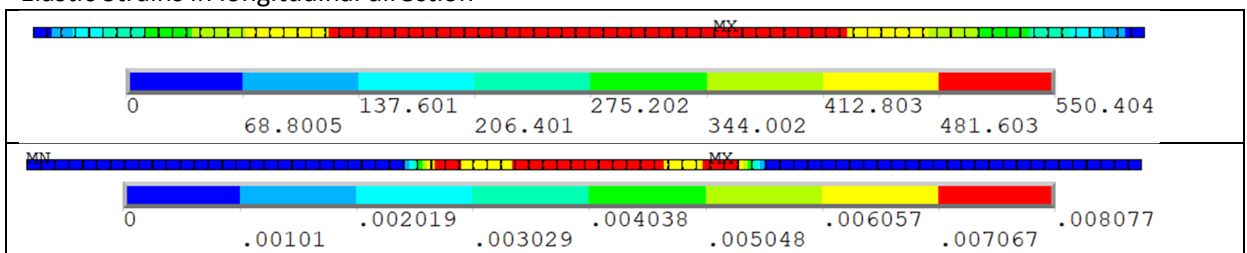

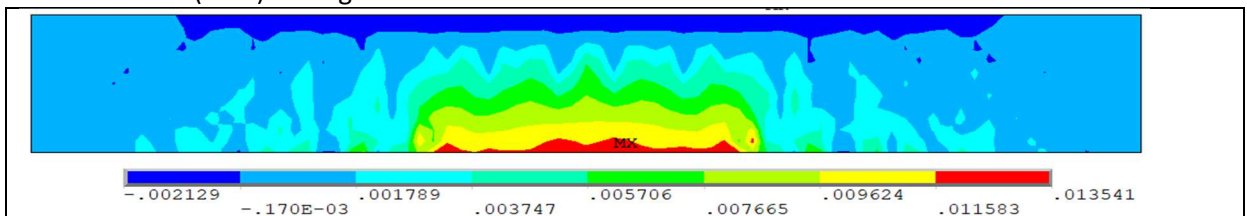Tensile Stress (MPa) in shear reinforcement
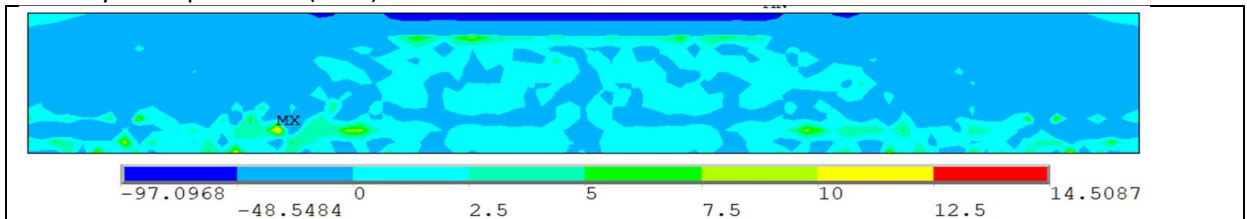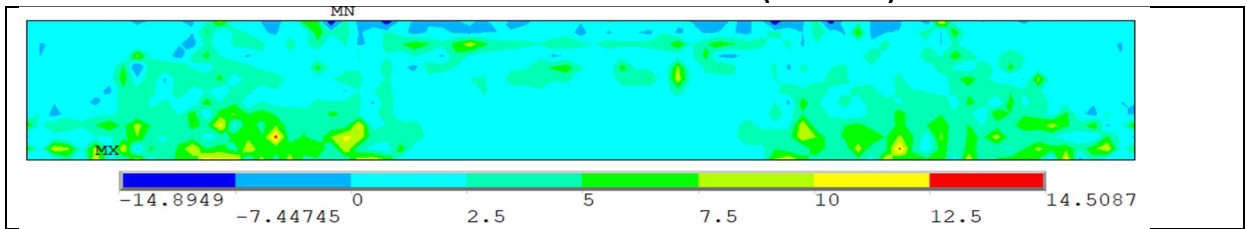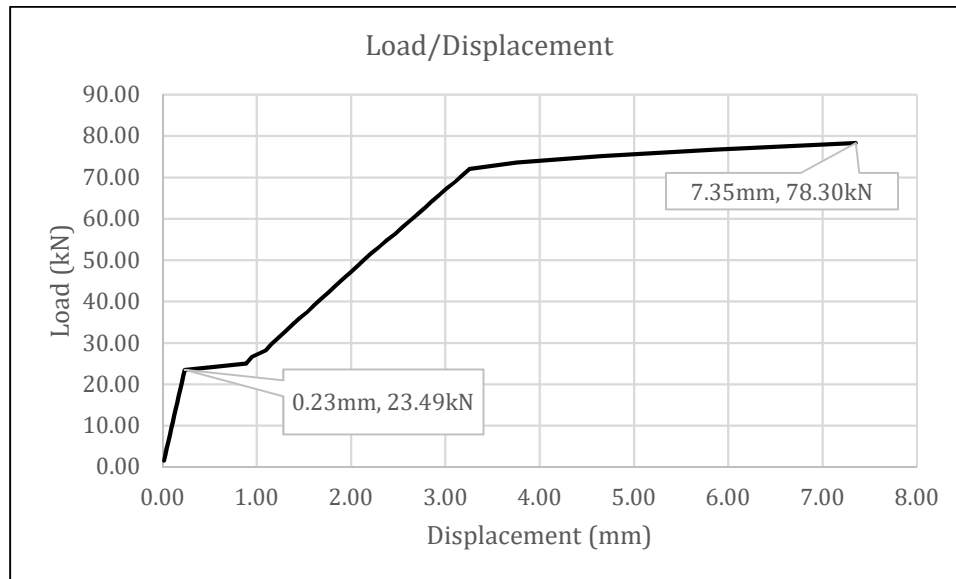

Simulated Crack Pattern

Figure 7.18 Plots: Hypothesis 2 - Test 3 – B10WS

Figure 7.19 Load/Displacement: Hypothesis 2 - Test 3 – B10WS

Results	Experimental	Simulated
Applied load (kN)	78.3	78.3
First crack load (kN)	10.0	23.49
Number of visible cracks	16	
Fracture type	Flexural	
Deflection midspan (mm)	14.23	7.35

Figure 7.20 Results: Hypothesis 2 - Test 3 – B10WS

7.3.7 Observations: Hypothesis 2 - Test 3 (Case B10WS)

- The simulated cracks go through the concrete in the part with shear forces. The stability of the beam is maintained by either the fibre model or the shear reinforcement.
- The main reinforcement has yielded.
- The plot for stresses in the shear reinforcement shows that stresses are transferred through the stirrups.
- Displacement is at 51% of reported value and the simulation has converged at max load.
- The flat area is present in the Load/Displacement diagram.

7.3.8 Results: Hypothesis 2 - Test 4 - B10WS (Fibre E = 22621)

HYPOTHESIS 2: CASE B10WS – LINEAR ELASTIC FIBRE MODEL (E = 22621)

Primary Principal Stress (MPa)

Normal Stress (MPa) in the longitudinal direction

Elastic Strains in the longitudinal direction

Tensile Stress (MPa) and Plastic Strain in the reinforcement

Compressive stress (MPa) in the top reinforcement

Tensile Stress (MPa) in the shear reinforcement

Simulated crack pattern
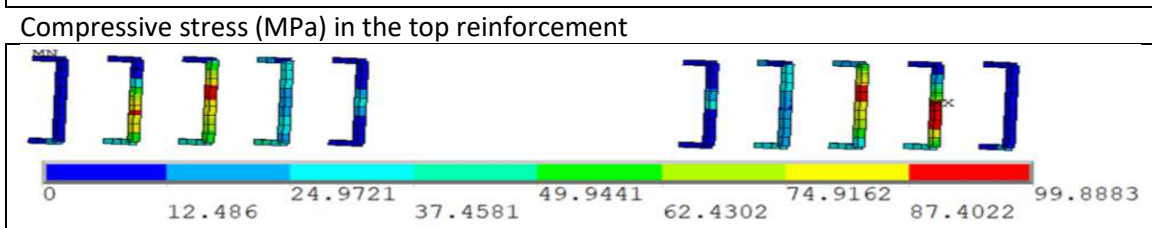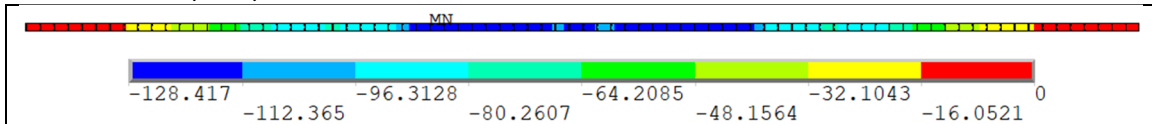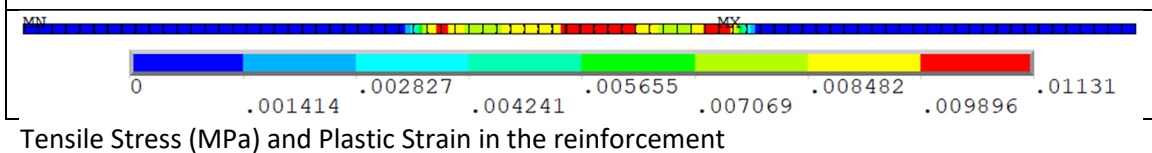
Figure 7.21 Plots: Hypothesis 2 - Test 4 - B10WS

Figure 7.22 Load/Displacement: Hypothesis 2 - Test 4 – B10WS

Results	Experimental	Simulated
Applied load (kN)	78.3	76.73
First crack load (kN)	10.0	23.49
Number of visible cracks	16	
Fracture type	Flexural	
Deflection midspan (mm)	14.23	8.34

Figure 7.23 Results: Hypothesis 2 - Test 4 – B10WS
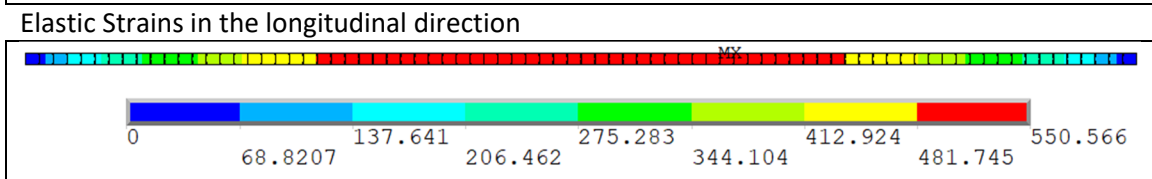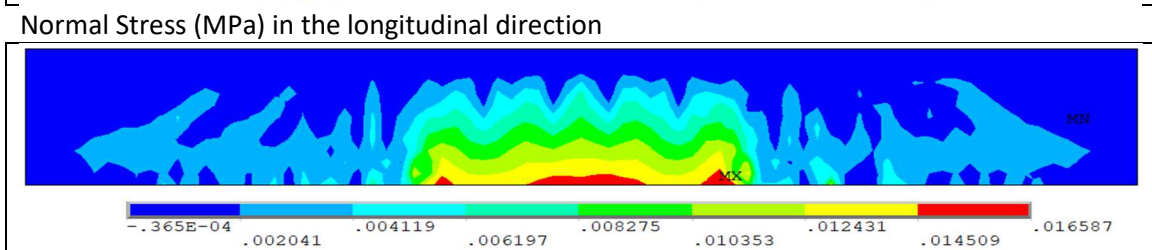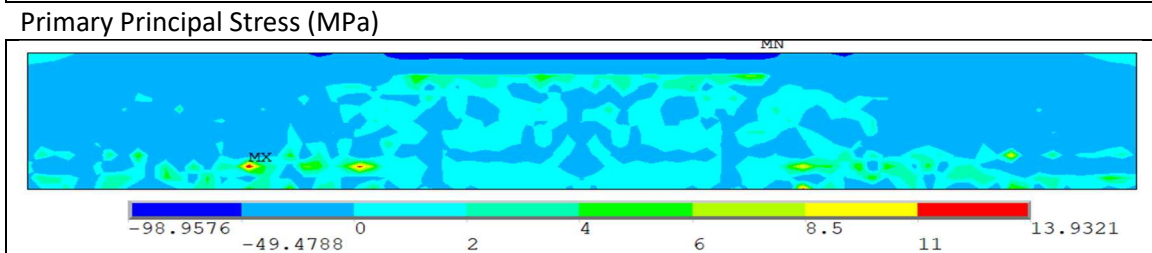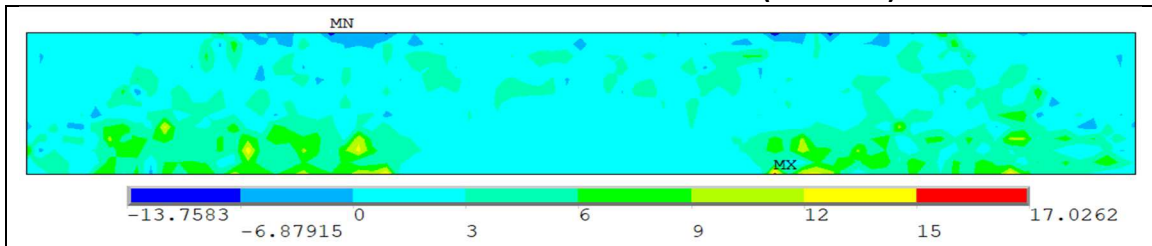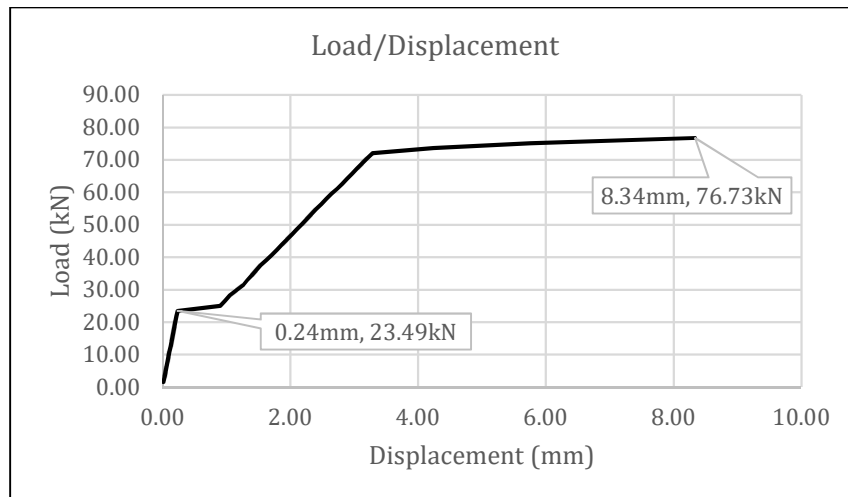
7.3.9 Observations: Hypothesis 2 - Test 4 (case B10WS)

- The cracks go through in this simulation as well.
- The main reinforcement has yielded
- The displacement is now at 58% of reported value. This must mean that reducing the E-modulus of the fibre influences the simulated behaviour of the concrete.
- The flat area is present in the Load/Displacement diagram.
- The applied load is 98% of maximum. See the note below.

The results above are for maximum load where the stability of the structure is maintained. The next substep of the simulation still converges, but there is a complete collapse of the concrete structure.
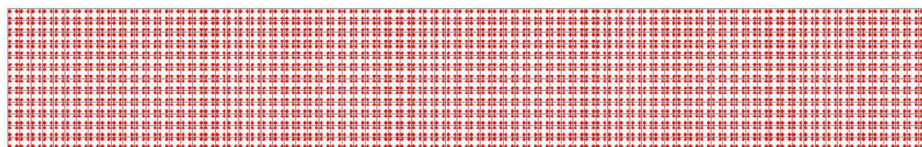
Figure 7.24   Crack plot at 100% load: Hypothesis 2 - Test 4 – B10WS

The reason that the simulation converges on a solution must be due to the fibre reinforcement model.

7.3.10 Intermediate conclusion: Hypothesis 2

The fibre models from the last hypothesis test were too simple and did not improve the accuracy of the simulations much. Further refining of the material models for fibre reinforcement is found to be beyond the scope of this thesis. The reasoning for this is found in the theory sub chapter 3.4 and, later, in chapter 8, "Discussion".

7.4 Hypothesis 3

It should be possible to model the post-crack behaviour of the concrete without modelling the fibres explicitly.

The SOLID65 element type does not allow any specific hardening/softening material model such as "kinematic-" or "isotropic hardening". At least, not to our knowledge. It is possible, however, to include a Drucker-Prager plasticity model. With this model, a flow rule and an accompanying elasto-plastic hardening rule can be established.

The values for cohesion and internal friction angle are calculated with the formulas from the theory chapter (formulas 3.3 - 3.6). For this method to work, the Drucker-Prager failure envelope must lie within the William-Warnke failure envelope (see the theory chapter, 3.9.4)

The flow rule is established with the angle of dilatancy. If this angle is equal to the internal frictional angle, the flow rule is associative. More about this in the theory chapter 3.5.2.

To observe changes in behaviour between an associative- and non-associative flow rule, two tests are run on both beams. The non-associative flow rule is defined by setting the angle of dilatancy to half of the internal friction angle.

Hypothesis:
The concrete material model in ANSYS combined with a Drucker-Prager plasticity model can predict the behaviour of the test cases

7.4.1 Test Setup

Setup	Structure	Element type	Material model	Material parameters	
Common	Beam	SOLID65	Linear isotropic	E-modulus (MPa)	45241
				Poisson's ratio	0.2
			Concrete	Open crack ratio	0.2
				Closed crack ratio	0.8
				Uniaxial cracking (MPa)	7.55
				Uniaxial crushing (MPa)	135
				Tensile relax. ratio	0.6
Test 1 Test 3			Drucker-Prager	Cohesion, C	9.39
				Int. friction angle, θ_f	58.9
				Angle of dilatancy, θ_d	58.9
Test 2 Test 4			Drucker-Prager	Cohesion, C	9.39
				Int. friction angle, θ_f	58.9
				Angle of dilatancy, θ_d	29.45

Figure 7.25 Test Setup: Hypothesis 3

7.4.2 Results: Hypothesis 3 - Test 1 - B10S (Associative Flow Rule)

HYPOTHESIS 3: CASE B10S – DP ASSOCIATIVE FLOW RULE ($\theta_d = \theta_f$)

Primary Principal Stress (MPa)

Normal Stress (MPa) in longitudinal direction

Elastic Strain in longitudinal direction

Plastic Strain in longitudinal direction

Tensile Stress (MPa) in reinforcement

Simulated crack pattern

Figure 7.26 Plots: Hypothesis 3 - test 1 – B10S

Figure 7.27   Load/Displacement: Hypothesis 3 - Test 1 – B10S

Results	Experimental	Simulated
Applied load (kN)	53.8	53.8
First crack load (kN)	12.9	22.6
Number of visible cracks	11	
Fracture type	Shear	
Deflection midspan (mm)	2.4	2.24

Figure 7.28   Results: Hypothesis 3 - Test 1 – B10S

7.4.3 Observations: Hypothesis 3 - Test 1 (case B10S)

There are several changes to the plots now with the Drucker-Prager plasticity included:

- The stress plots appear smoother and have a more reasonable maximum stress.
- The areas of maximum stress are larger.
- There is a jump in the flat area in the Load/Displacement diagram (noted by the light red callout).
- There are now small plastic strains in the concrete due to the implemented flow- and hardening rule.

Additional observations:

- The deflection is at 93% of the reported values.
- The simulation still converges at max load.

7.4.4 Results: Hypothesis 3 - Test 2 - B10S (Non-Associative Flow Rule)

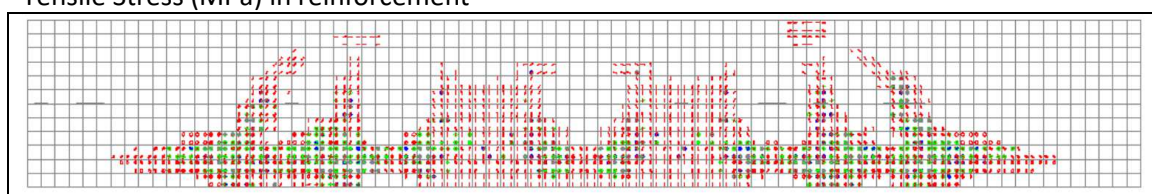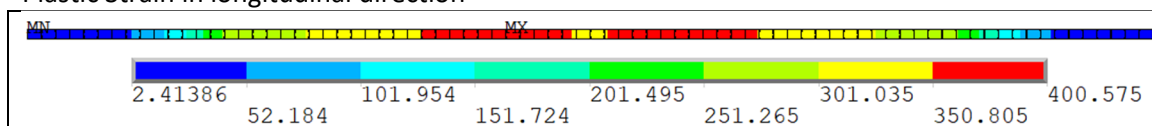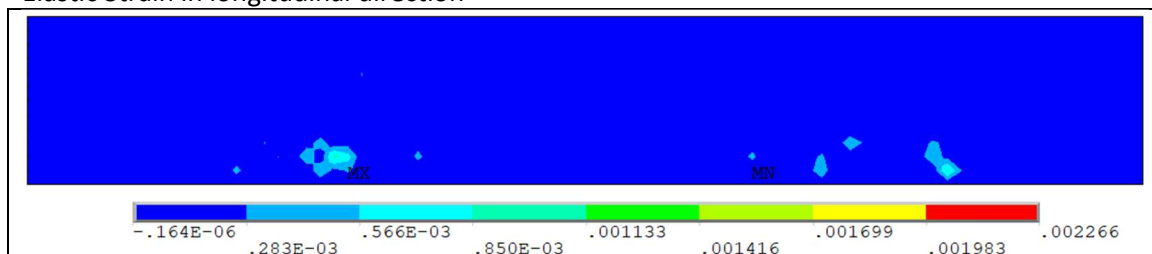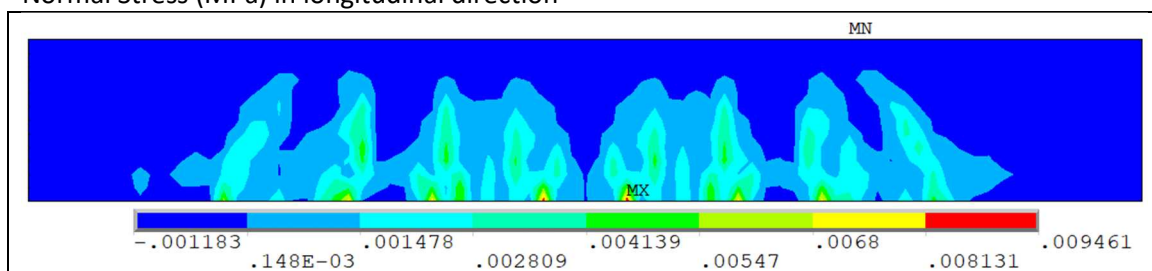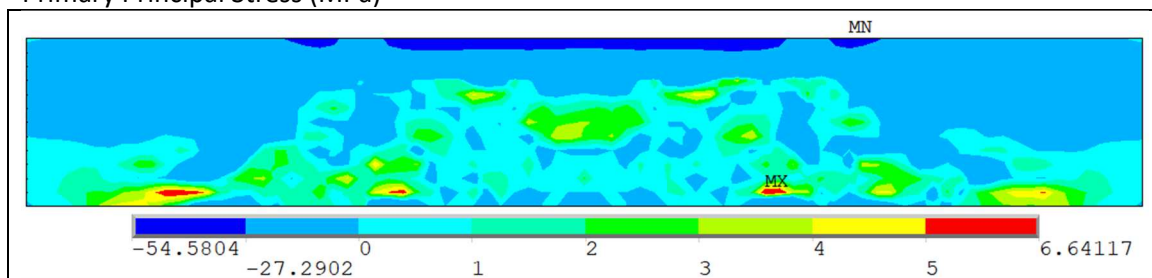**HYPOTHESIS 3: CASE B10S – DP NON-ASSOCIATIVE FLOW RULE ($\theta_d = 0.5 \cdot \theta_f$)**

Primary Principal Stress (MPa)

Normal Stress (MPa) in longitudinal direction

Elastic Strain in longitudinal direction

Plastic Strain in longitudinal direction

Tensile Stress (MPa) in reinforcement
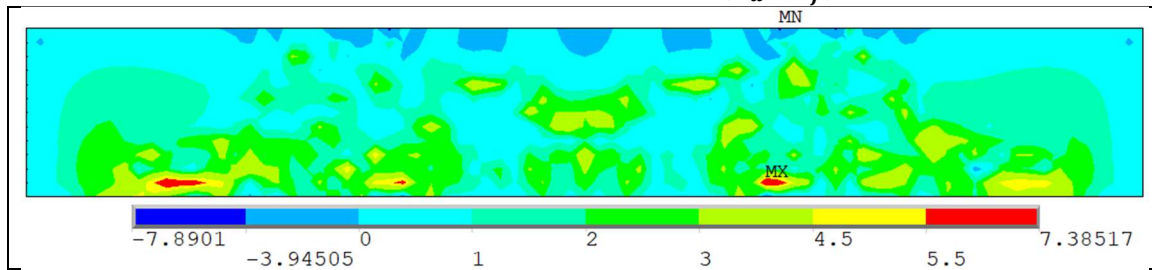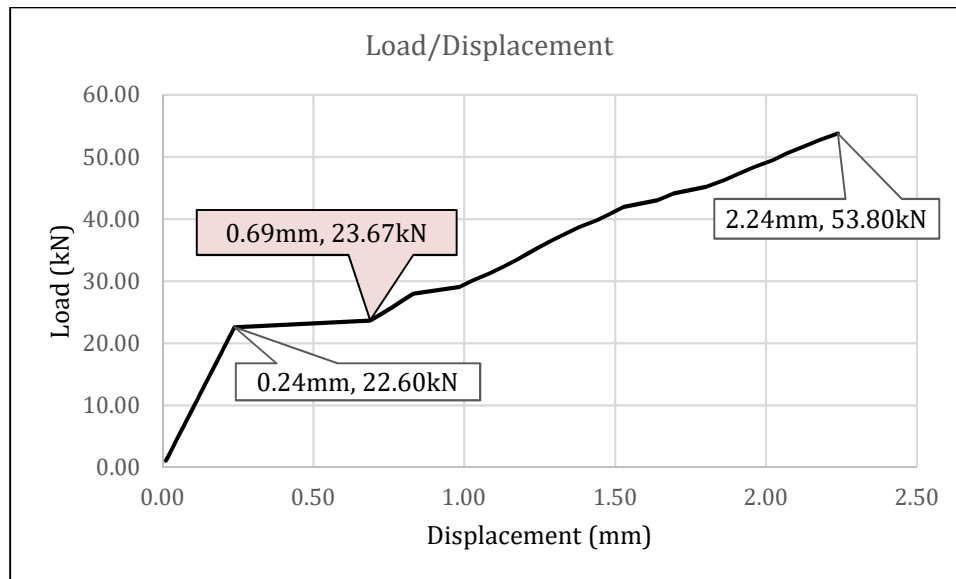

Simulated crack pattern

Figure 7.29 Plots: Hypothesis 3 - test 2 – B10S

Figure 7.30 Load/Displacement: Hypothesis 3 - Test 2 – B10S

Results	Experimental	Simulated
Applied load (kN)	53.8	53.8
First crack load (kN)	12.9	22.6
Number of visible cracks	11	
Fracture type	Shear	
Deflection midspan (mm)	2.4	1.95

Figure 7.31   Results: Hypothesis 3 - Test 2 – B10S

7.4.5 Observations: Hypothesis 3 - Test 2 (Case B10S)

- With the Drucker-Prager with non-associative flow, the curve in the Load/Displacement diagram has been smoothed out. There are still differences to the experimental data, but this is another step in the right direction.
- The reduced flow leads to reduced deflection and it is now at 81%.
- There are large uncracked areas closer to the supports. This indicates that the shear strength is overestimated in this simulation.
- The maximum stresses are still close to tensile strength.

7.4.6 Results: Hypothesis 3 - Test 3 - B10WS (Associative Flow Rule)

HYPOTHESIS 3: CASE B10WS – DP ASSOCIATIVE FLOW RULE ($\theta_d = \theta_f$)
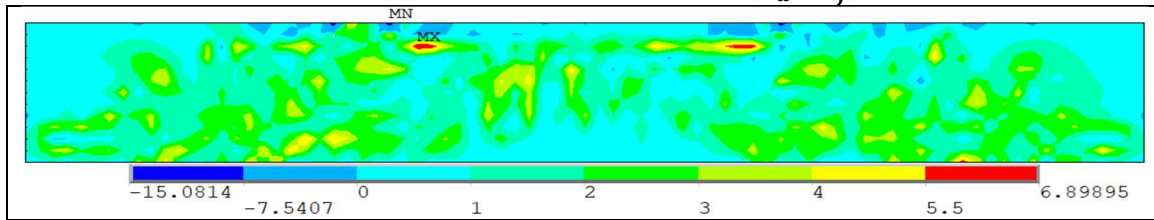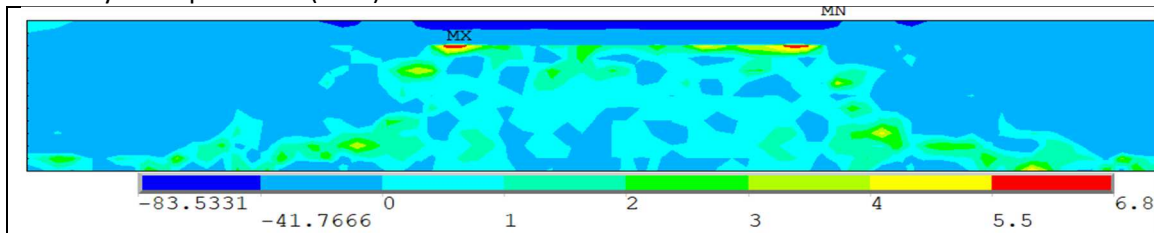
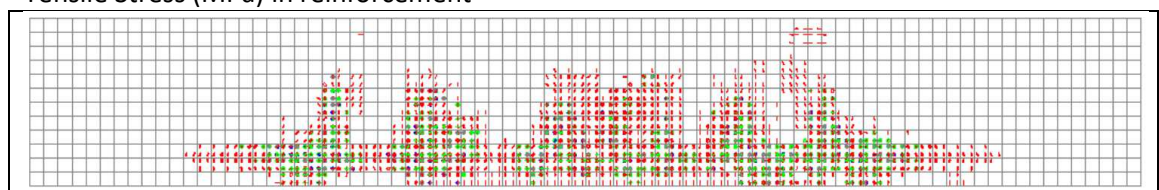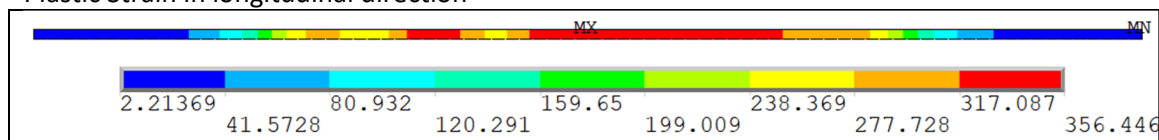Primary Principal Stress (MPa)

Normal Stress (MPa) in longitudinal direction
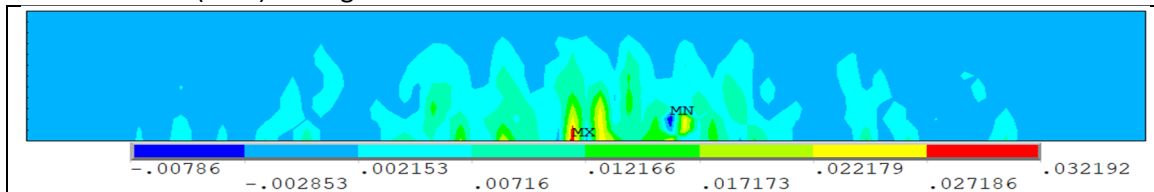
Elastic Strain in longitudinal direction
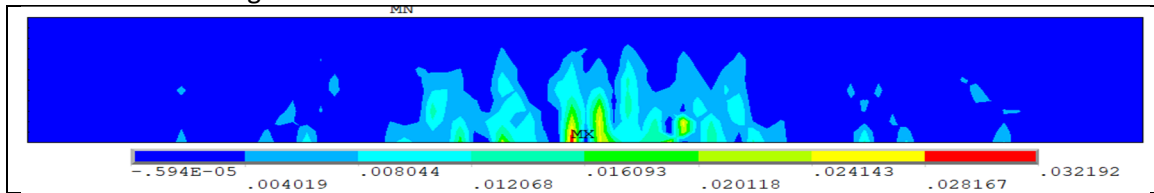
Plastic Strain in longitudinal direction
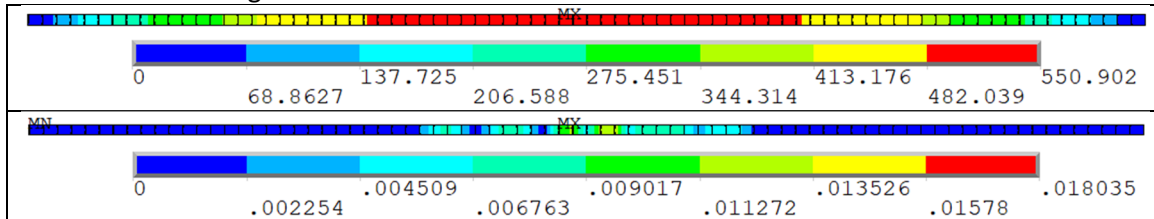
Tensile Stress (MPa) and Plastic Strain in the reinforcement
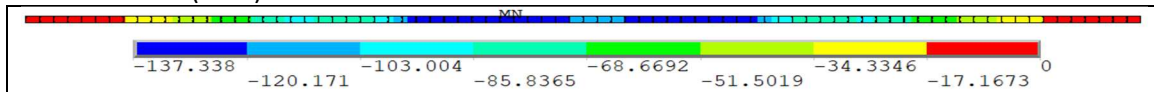
Compressive Strength (MPa) in the top reinforcement
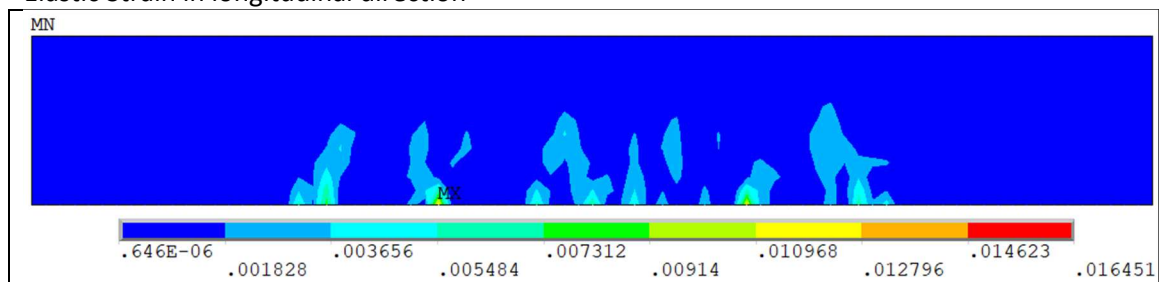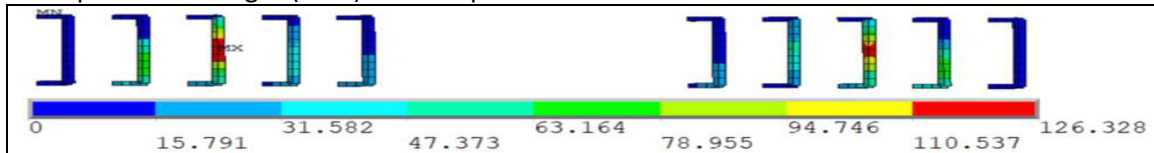

Tensile Stress (MPa) in shear reinforcement
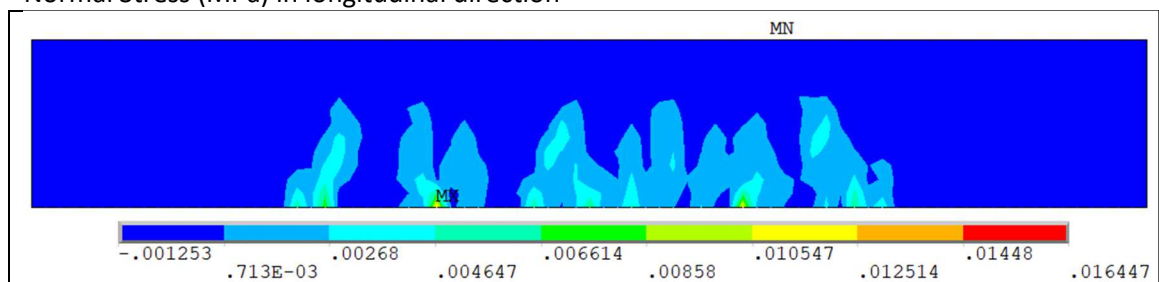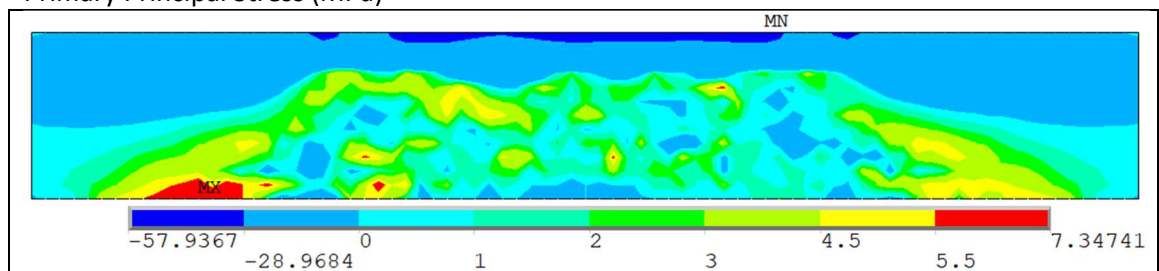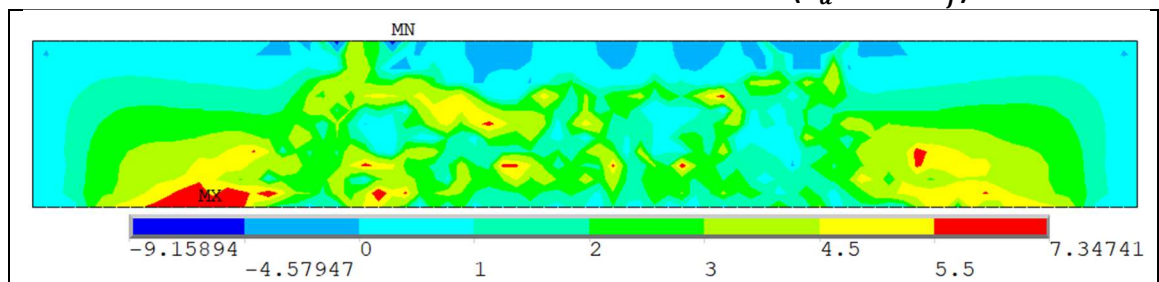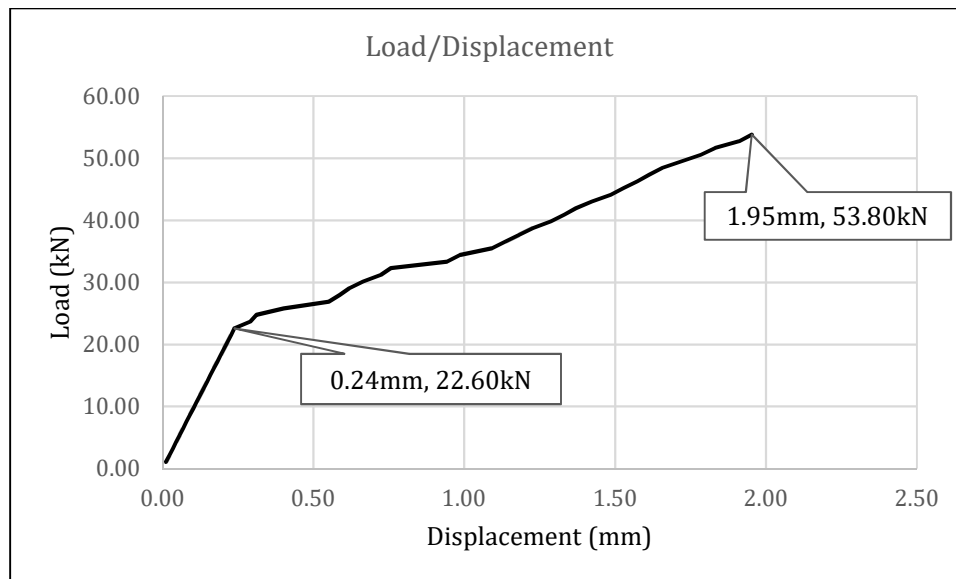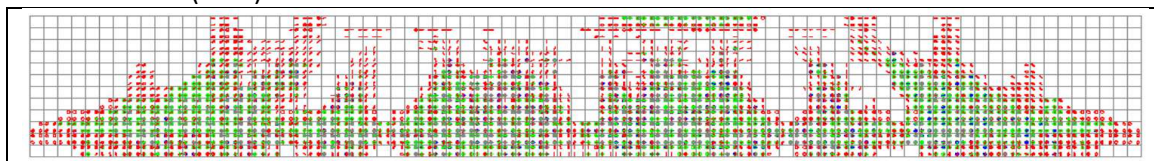

Simulated crack pattern

Figure 7.32 Plots: Hypothesis 3 - Test 3 – B10WS
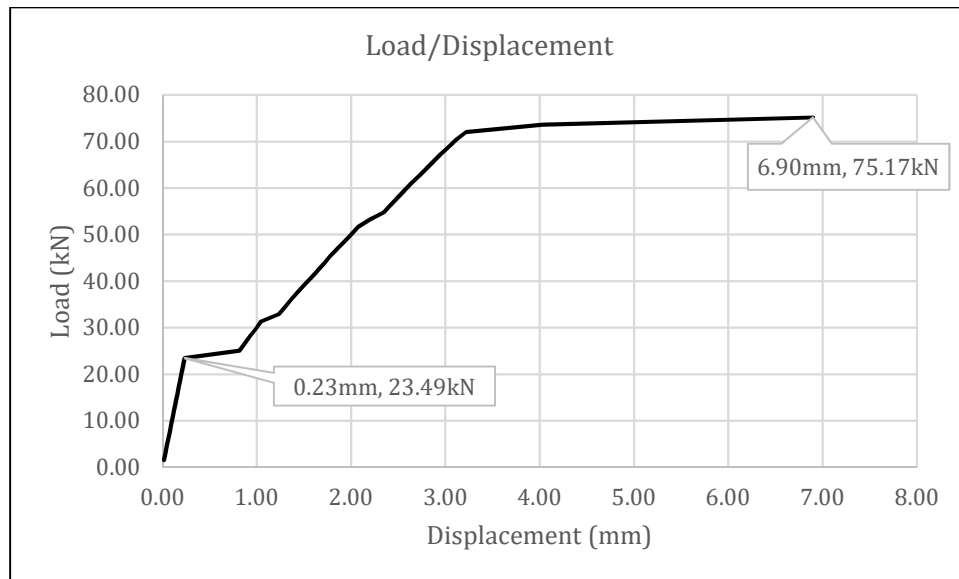
Figure 7.33   Load/Displacement: Hypothesis 3 - Test 3 – B10WS

Results	Experimental	Simulated
Applied load (kN)	78.3	75.17
First crack load (kN)	10.0	23.49
Number of visible cracks	16	
Fracture type	Flexural	Flexural
Deflection midspan (mm)	14.23	6.9

Figure 7.34 Results: Hypothesis 3 - Test 3 – B10WS

7.4.7 Observations: Hypothesis 3 - Test 3 (Case B10WS)

- The simulation of this beam also yields smoother stress plots.
- There is yielding in the main reinforcement
- The maximum stresses are a little below tensile strength
- The platform after cracking has a visible slope
- Deflection is at 48%
- Simulation stops converging at 96% load with flexural fracture

7.4.8 Results: Hypothesis 3 – Test 4 - B10WS (Non-Associative Flow Rule)

HYPOTHESIS 3: CASE B10WS – DP NON-ASSOCIATIVE FLOW RULE ($\theta_d = 0.5 \cdot \theta_f$)

Primary Principal Stress (MPa)

Normal Stress (MPa) in longitudinal direction

Elastic Strain in longitudinal direction

Plastic Strain in longitudinal direction

Tensile Stress (MPa) and in the bottom reinforcement

Compressive Stress (MPa) in the top reinforcement

Tensile Stress (MPa) in the shear reinforcement

Simulated crack pattern
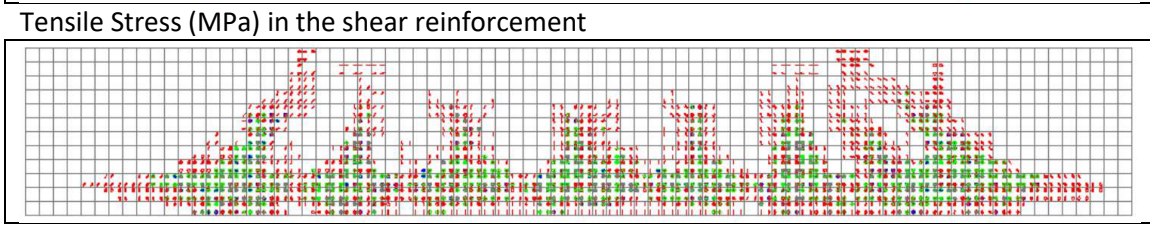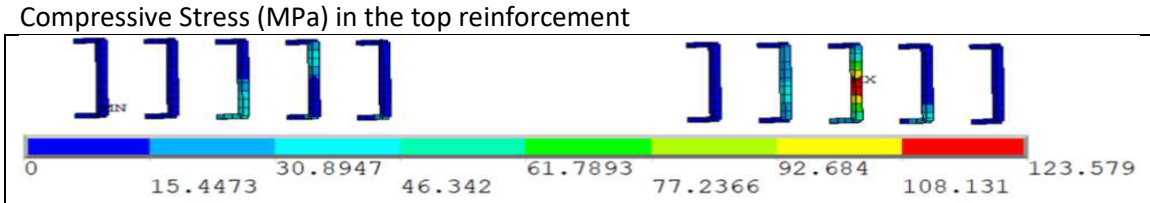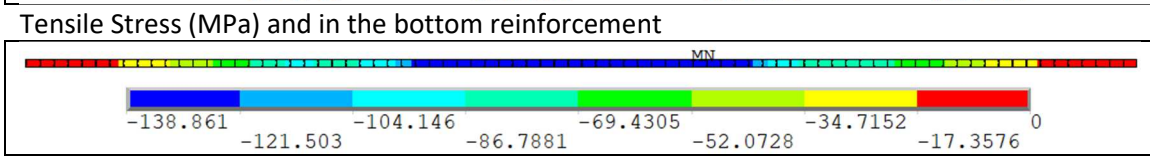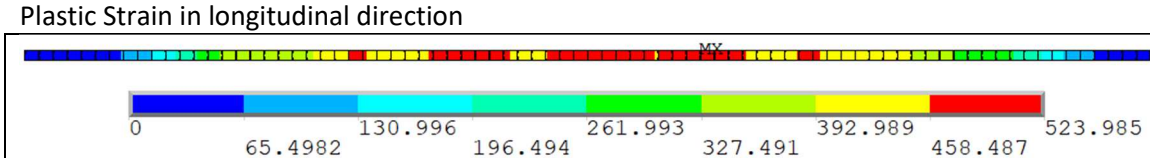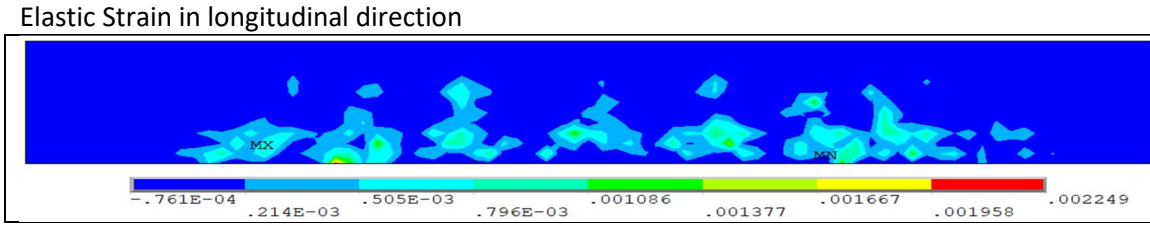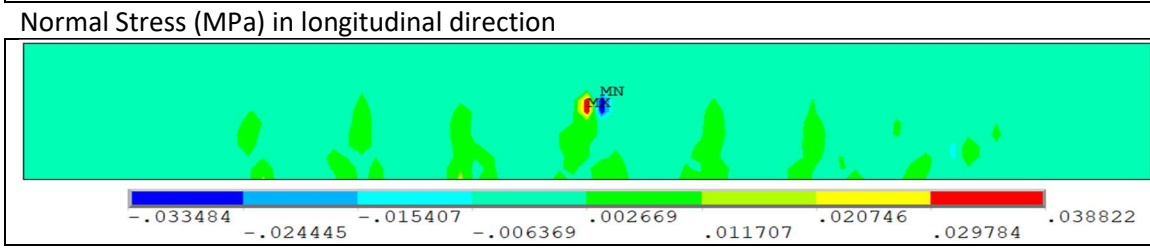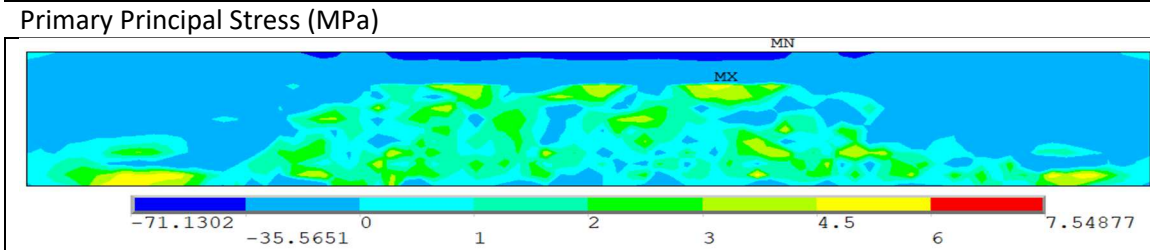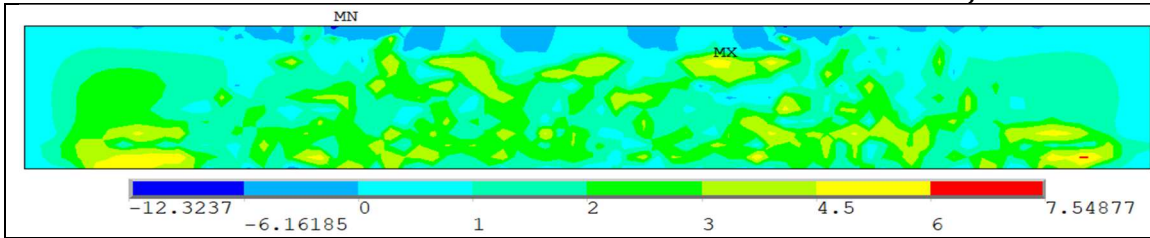
Figure 7.35 Plots: Hypothesis 3 - Test 4 – B10WS
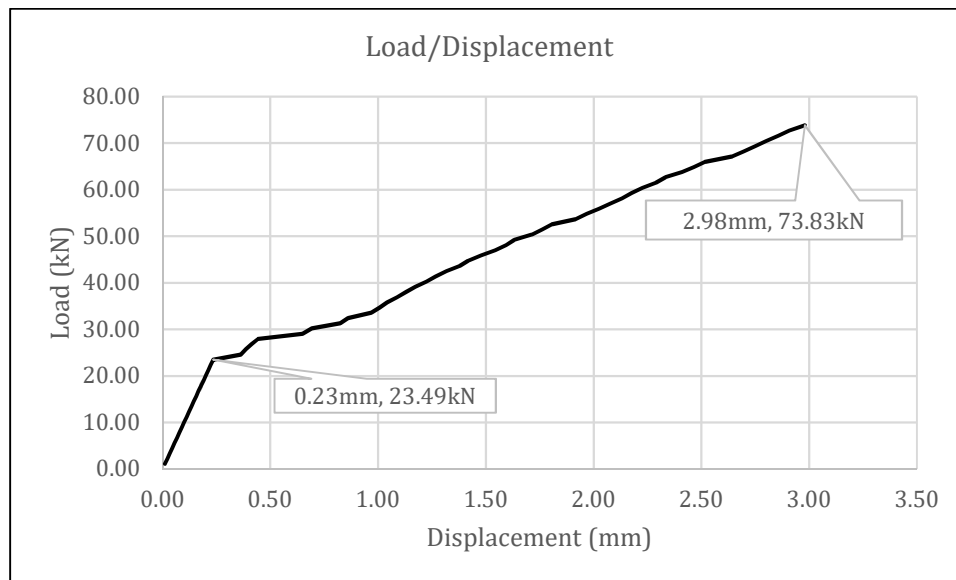
Figure 7.36 Load/Displacement: Hypothesis 3 - Test 4 – B10WS

Results	Experimental	Simulated
Applied load (kN)	78.3	73.83
First crack load (kN)	10.0	23.49
Number of visible cracks	16	
Fracture type	Flexural	Shear
Deflection midspan (mm)	14.23	2.98

Figure 7.37 Results: Hypothesis 3 - Test 4 – B10WS

7.4.9 Observations: Hypothesis 3 - Test 4 (Case B10WS)

- The transition in smoothed in the post crack area.
- The maximum tensile stresses are close to tensile strength
- The main reinforcement has not reached yielding stress which leads to small displacement
- The simulation stops at maximum 94% load with fracture due to tensile stress from the shear forces

7.5 Comparison of Load/Displacement curves from the hypothesis tests

The curves in the graphs below are named according to the hypothesis and test number. E.g. test 2 from hypothesis 3 will be "H3 T2"

		Material model	Case	Curve
Hypothesis 1		Concrete model alone	B10S	H1 T1
			B10WS	H1 T2
Hypothesis 2		Smeared reinf. E = 45241	B10S	H2 T1
			B10WS	H2 T3
		Smeared reinf. E = 22621	B10S	H2 T2
			B10WS	H2 T4
Hypothesis 3		Drucker-Prager Ass.	B10S	H3 T1
			B10WS	H3 T3
		Drucker-Prager Non-Ass.	B10S	H3 T2
			B10WS	H3 T4

Figure 7.38 Identification of graph legend
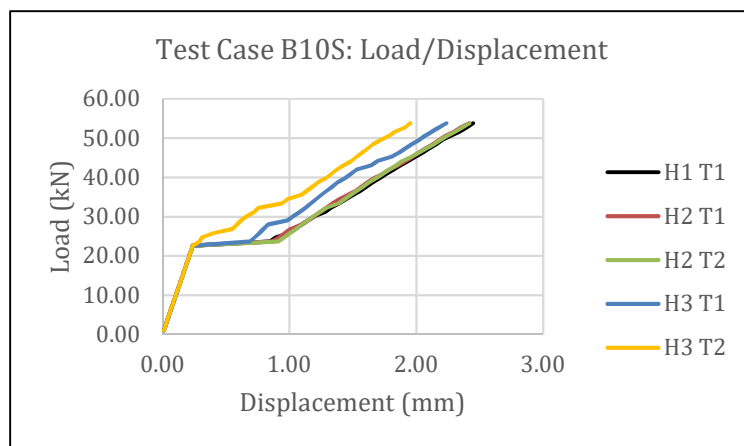
Figure 7.40 Load/Displacement: Test Case B10S
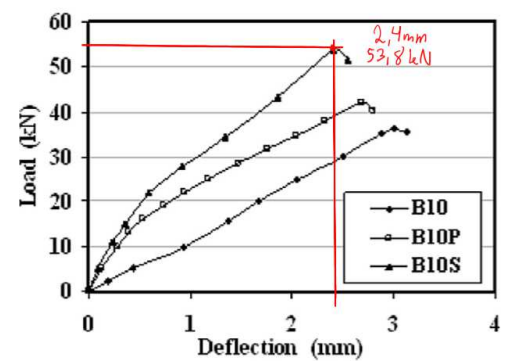
Figure 7.39 Experimental data B10S
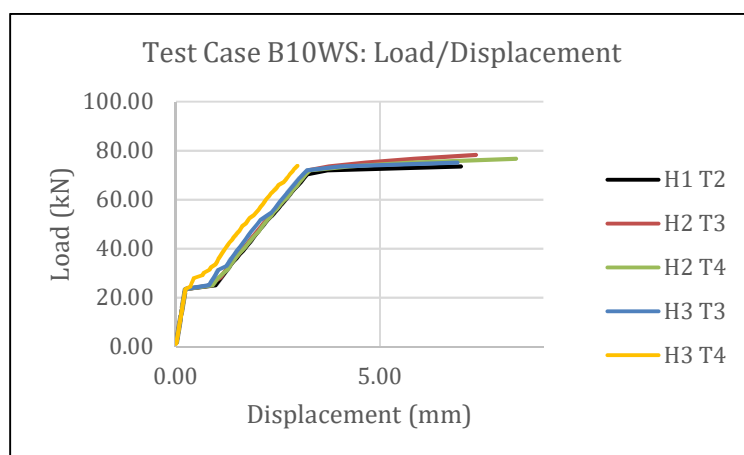
Figure 7.42 Load/Displacement: Test Case B10WS
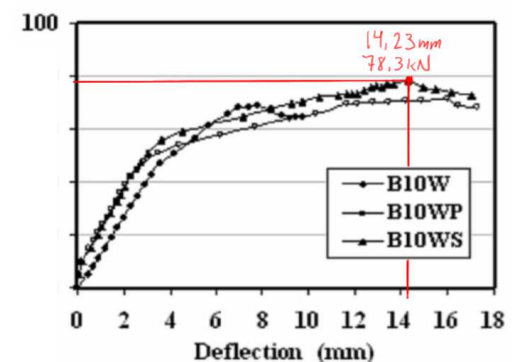
Figure 7.41 Experimental data B10WS

Note that for B10WS, every curve except H3 T4 moves towards an asymptote closer to maximum load. This must be where yielding in the bottom reinforcement occurs.

None of the tests for B10S reach non-convergence of the solution. For B10WS only the tests with the simple fibre model reached non-convergence

8 Discussion

A discussion of the test results is presented in this chapter. The text follows the same structure as the test results, where the hypotheses are presented in consecutive order. The discussion about each hypothesis builds on the information from the previous one.

8.1 Initial remarks on the work presented in this report

The results are divided into groups corresponding to our hypotheses. The three main hypotheses presented in the result chapter are meant to represent the findings of all our work. Many more tests have been carried out and the results from these tests are used to revise the theories presented in the theory chapter and the ANSYS workflow presented in the method chapter. This way of presenting the work can be understood from our research strategy. This entire report is based on knowledge gained from the iterative process of the hypothetico-deductive method.

8.1.1 General restrictions, simplifications and assumptions for the tests in ANSYS

First off, we are running the tests on the student version of ANSYS. There are restrictions to the number of nodes and elements we can use to mesh the beams.

The structural model in ANSYS is not exactly modelled as the experimental beams. The original report is a little unclear as to where the point loads from the testing machine are located. There is no information on the size of the concrete cover. The number of stirrups used in the original experiment do not match the shear reinforced part of the beam and the stirrup spacing. We have modelled an approximately correct beam for our tests.

Only the compressive strength of the concrete is known from the original experiments. Values for e-modulus, Poisson's ratio and tensile strength are derived from other sources.

All the above can cause inaccuracies in the simulations.

8.2 Discussion on the hypothesis tests

The William-Warnke model used in ANSYS is a modified form of the original yield criterion. Instead of being continuous, the yield surface is cut at regions with tensile stresses. This is best explained with the figure from the theory chapter:
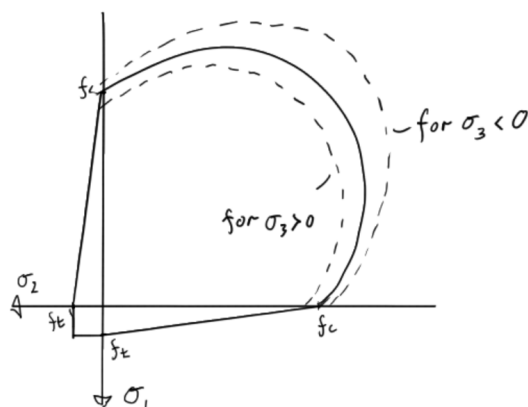
Figure 8.1   Biaxial yield envelope for the concrete material model in ANSYS

First off, this is probably a reasonable simplification for normal concrete structures where the tensile strength of the concrete is small and usually neglected. Small differences in multiaxial strength will not have a major impact on the solutions. This should also be true for UHPFRC because the tensile- to compressive strength ratio of the material is often lower than that of normal concrete. In this regard, the simplifications of the William-Warnke model could be reasonable.

In the next section of this chapter we will go through the hypotheses and their test results. For convenience, a quick recap of the hypotheses and the test setups is provided below.

Hypothesis 1: The concrete material model in ANSYS alone can predict the behaviour of the test cases.
The beams are tested once.
Hypothesis 2: The concrete material model in ANSYS combined with a fiber model can predict the behaviour of the test cases.
Smeared reinforcement is used for the element SOLID65 to simulate fibres. The material model for the reinforcement is linear elastic only. The beams are tested twice, with the first one having an E-modulus for the fibre of E = 45241MPa. The second test is with E = 22621MPa
Hypothesis 3: The concrete material model in ANSYS combined with a Drucker-Prager plasticity model can predict the behaviour of the test cases.
The concrete model is combined with a Drucker-Prager plasticity model. Both beams are tested twice. The first test is with an associative flow rule and the second test is with a non-associative flow rule.

Figure 8.2 Overview of the discussion of the hypothesis tests

8.2.2 Hypothesis 1

Our initial assumption was that the William-Warnke based concrete model in ANSYS would be enough to predict the behaviour of simple UHPFRC beams. This assumption has been a major part of our work. We imagined that if the ready-made material model for concrete could represent UHPFRC adequately, we could design and analyse almost any structure. As the saying goes; "There is no need to reinvent the wheel."

The first hypothesis is built on this initial assumption. The results from the tests indicate that this is not entirely true. It is a step further from a linear elastic analysis and gives indications on where cracks are likely to initiate.

One of the key features of UHPFRC is its ability to transfer stresses over cracks via the fibre reinforcement. This should allow for designing structures with reduced amount of normal reinforcement.

The behaviour of the load/displacement curve, and thereby the stress/strain relationship, must be under our control. The reason being that the formation of stress concentrations and cracks are dependent on the ability of the material to deform and redistribute stresses.

The load/displacement curves of the first hypothesis tests are not the same as those found in the laboratory experiment. After cracking, large strains occur without a significant increase in stress. This is curious. We think this happens because the cracked components of the element stiffness matrices are severely reduced. The stresses will immediately be redistributed to nearby elements and cause stress concentrations there. With this, the crack propagation will be very fast unless restrained by the normal reinforcement. Between the load steps the load is increased by 2%. Since the concrete model does not have plastic behaviour, the cracks will fill a rather large area just with this small increase in load. This leads to reduction in the stiffness matrix for the entire beam with rather large displacement before the reinforcement counteracts this on the next loadstep.

The beams were analysed with a simplification of the behaviour of the fibre reinforcement. We assumed that the fibres were isotropically oriented and packed and solely represented by the tensile strength. This is very seldom the case in a real structure and will most likely lead to inaccuracies in the analysis.

We also assumed that the multiaxial compressive behaviour of the concrete would have little impact on the results from the tests. The concrete material model allows specification of this behaviour, but we left it with the default values. In the theory chapter, we found that for UHPFRC's with low volume fractions of fibre can have reduced strength in biaxial compression. Especially if the stresses in each direction are close to equal. Certainly, there are areas in the tested beams that are exposed to both biaxial and triaxial compression and the beams contain only 0.5% volume fraction of fibres.

8.2.3 Tests for hypothesis 1

The results from test case B10S reveal that the material model overestimates the shear strength of the concrete. The deflection, however, is very close to what is reported in the original report on the test. We believe that the reinforcement is what provides the most stiffness in the tensile region of the beam and, by that, gives the beam it's flexural performance.

The crack plots do not indicate whether the fracture will be from shear force or from moment. We can assume that the reinforcement still constrains crack propagation caused by the moment. In this case, an increase in load will lead to shear fracture. Another indication of this is the 2nd cracks that appear. In the areas with shear forces, these cracks are closer to the top of the beam than those found in areas with the largest moment. This could mean a higher chance of shear fracture.

The simulations for test case B10WS stops converging at loads just below reported fracture load. This must be due to the inclusion of shear reinforcement and compression reinforcement. This leads to an understanding that the concrete material model can, to an extent, predict the behaviour of shear reinforced UHPFRC beams.

The predicted deflection is smaller than the experimental data. This must be attributed to the inaccuracies in the model. When the reinforcement yields, large strain occur with small increase in stress. But, the cracks continue to grow and will quickly go through the cross section. It is difficult to model this accurately since the concrete model has no ductile behaviour.

All tests done for this hypothesis have small areas in the stress plots where the tensile stress is considerably larger than the tensile strength. It is unclear what causes this. An idea is that the increase in load between substeps in the simulation is 2%. This "jump" in loading can maybe cause these high stress concentrations before cracking checks are done. In this case, the phenomenon is an artifact of the finite element simulation and not a physical reality.

8.2.3 Hypothesis 2

We hypothesized that by explicitly modelling the behaviour of the fibres in the UHPFRC, we could control the behaviour of the deforming material better.

From the theory we recall that the influence of the fibers can be described by an efficiency factor. This factor takes the orientation and the local volume fraction of the fibres into account. These two properties are explained by the rheological properties of the concrete, the casting procedures, the characteristics of the casting mould and the mechanical properties of the fibres. We understand that this quickly lead to many variables that needs to be addressed.

The information in the report on the experimental beam tests only gives clues about the characteristics of the casting mould and the properties of the fibres. We could set arbitrary values for all the variables and define a hypothetical efficiency factor. Then there is the issue of modelling this for use in ANSYS. This would lead to much guesswork and the trustworthiness of the simulation results would not improve. Eventually we stopped delving deeper and determined that the intricacies of this subject are outside the scope of this Master thesis.

Still, we wanted to use a very simplified model to simulate the behaviour of the fibres. The SOLID65 element can contain smeared reinforcement. This reinforcement is defined by orientation and volume fraction, akin to the fibre efficiency factor. The simplest material model was assigned to the smeared reinforcement and the orientation and local volume fraction was assumed to be uniform.

8.2.4 Tests for hypothesis 2

For comparison reasons, two different E-moduli were given to the material model for the fibre reinforcement.

The test results for test case B10S show almost the same as the results from hypothesis 1. The deflection is slightly lower with the inclusion of the fibre model. This must be ascribed to the added strength from the fibre model.

The simulations for both tests for test case B10WS converge on a solution. It becomes clear that the included smeared reinforcement is capable of bridging cracks. This can especially be seen in the results and observations for test 4. The crack plot evolves like we have been used to up until the last substep of the simulation. In the last substep, suddenly all concrete elements are marked as being crushed. We know that the smeared reinforcement is activated after cracking or crushing has been simulated. This means that the structural stability now depends on the grid of smeared reinforcement which is activated in the entire beam. While this is not a representation of reality, it is, nonetheless, an interesting result.

The material model chosen for the smeared reinforcement only describes linear elastic behaviour. Since no yielding of the material has been prescribed, it has unlimited strength. The only limiting factor is the built-in displacement controls in ANSYS. The simulation will stop if a very high displacement occurs, regardless of the convergence tolerance or material properties. This usually only happens if the stability of the structure is compromised which will lead to rigid-body movement.

8.2.4 Hypothesis 3

If we assume that the post-yield behaviour is an inherent part of the concrete, we can try to model this directly by determining a flow rule and an accompanying hardening rule. These rules, or functions, define how the concrete flows after yielding and how the yield surface changes with increasing strains. This is often connected to the function of the yield surface, especially for associative flow rules. The general form of the flow rule is displayed below for reference:

$$d\varepsilon_p = \lambda \cdot \frac{dQ}{d\sigma_{ij}}$$

Q is the flow potential and is equal to the function of the yield surface if the flow rule is associative. It is obviously a benefit if the function for the yield surface is continuous due to the differentiation involved. Especially so, if the yield function is complicated, such as the William-Warnke criterion.

The tension "cut-off" for the William-Warnke model in ANSYS presents a challenge when deriving flow- and hardening rules due to the discontinuity of the yield surface. This may be one of the reasons why the model is so restricting when it comes to defining post-yield characteristics.

In ANSYS, we have only found one material model capable of controlling the post-yield behaviour of the SOLID65 elements. This is the Drucker-Prager plasticity model. The model is easier to handle than the William-Warnke model and is implemented in ANSYS without simplifications. The model can handle both a flow rule and a hardening rule, although the latter is fixed to be of an elasto-plastic type. The flow rule is defined via the angle of dilatancy.

For the combination of William-Warnke yielding and Drucker-Prager flow to work, the Drucker-Prager yield surface must lie within the yield surface of William-Warnke. The reason being that the flow rule should not be activated until after yielding, defined by the William-Warnke model. This will produce some obvious inaccuracies in the areas where there are larger differences between the yield surfaces. For concrete structures that mainly fails due to tensile stresses, the differences should be smaller due to shape of the two yield criterions.

For the tests in hypothesis 3, we used two flow rules. One with an angle of dilatancy equal to the internal frictional angle and the other with a halving of the angle of dilatancy (I.e. one with an associative flow rule and one with a non-associative flow rule).

8.2.5 Tests for hypothesis 3

The use of the Drucker-Prager plasticity model produced some interesting results. At a glance, the tensile stress areas appeared much smoother than for the earlier tests. This could be ascribed to the plasticity of the concrete. Tensile stresses will now wax, and wane rather than immediately disappear at yielding. The maximum values of the tensile stresses are also close to the tensile strength of the concrete. This is a better representation of the real behaviour of the UHPFRC beams.

This effect also influences the load/displacement curve, which is more smoothed compared with previous tests. This is more pronounced in the material model with the non-associative flow rule. The smoother curves are more in line with the load/deflection curves from the original experiments.

The test results for test case B10S generally shows an overestimation of the shear strength of the material. However, with increasing loads, the test with an associative flow rule could tend to show that the beam will fail in shear.

Further indications for this can be seen in the stress plot for the reinforcement. The tensile stresses near the middle of the reinforcement are reduced. This means that more of the stresses have been redistributed to the sides of the beam and will likely increase shear stresses. Since the area with shear forces is not reinforced, this is a likely place cracks will propagate and meet the cracks that has now appeared just below the point loads. Out of all the B10S tests, this is the closest one to get a shear fracture which is what is reported in the original experiment.

With a non-associative rule, the shear strength and the stiffness of the B10S beams is further increased. The stiffness increase can be attributed to the reduced strain rate of the material which has eliminated the flat area in the Load/displacement diagram.

The test results for test case B10WS both stop converging at loads close to maximum. The test, where the concrete model has an associative flow rule, has a flexural type of fracture and the deflection is large compared with the other tests. For the beam with a non-associative flow rule, the deflection is very small because the reinforcement hasn't reached yielding stress. The fracture in this beam is from shear forces.

The most important result of this test, however, is the smoother load/displacement diagram. We believe that this is a step in the right direction for the task of describing and modelling the behaviour of UHPFRC. The next step is to implement a hardening/softening-rule, but the concrete material model in ANSYS and the element type SOLID65 are inflexible in this regard.

8.3 Summary of the discussion on the hypothesis tests

We cannot, for certain, draw a conclusion that any of the proposed material models is close to representing the real material behaviour of UHPFRC. The reason why many of the tests show similarities with the experimental data is because the beams are reinforced. Thus, the most interesting test results, in our opinion, are the ones from hypothesis 3 with the Drucker-Prager plasticity model. The reason why these are interesting is that they show a post-crack behaviour more akin to what we would've expected from a fibre-reinforced concrete.

8.3 Discussion on the choice of method

To get started with the work in ANSYS we decided to use test cases from research outside the University of Agder. We could have tested beams ourselves, but we decided against it because of limited capacity in the laboratory this spring. In addition to this, if beams were to be made by us, the thesis would likely have been shifted towards mix proportioning and beam design to standards. We wanted to have a deeper look into the behaviour of UHPFRC and we are certain that the work we have done with ANSYS and the material models leads us in the right direction.

We decided to only use material models readily available to us through the graphical user interface in ANSYS. We believed it would shift our focus away from studying the behaviour of UHPFRC if we had to learn the APDL-language and the necessary coding abilities.

UNIVERSITETET I AGDER

9 Conclusion

The research question:

How can we analyse UHPFRC beams with the help of ANSYS?

How does the built in concrete material model in ANSYS work?

How can the concrete material model in ANSYS simulate behaviour of UHPFRC beams?

The concrete material model in ANSYS is based on K. J. William and E. P. Warnke's 5-parameter constitutive model for triaxial behaviour of concrete. The yield surface described in the original article is only activated for concrete under triaxial compression. In biaxial compression, the failure surface is adjusted for the magnitude of the tensile stress in the normal direction. The response of concrete in biaxial and triaxial tensile stress is simplified. For biaxial tension the failure surface is defined as a linear relationship between compressive and tensile strength. For pure tension, a Rankine type of yield criterion is assumed.

The concrete model in ANSYS works in conjunction with the element type SOLID65. This element type can simulate cracking and crushing of the concrete. This is done by reducing components in the stiffness matrix to a low value. The stresses are then redistributed to the stiffer nearby elements. This redistribution causes stress concentrations which facilitate more cracking and will, by this, simulate crack propagation in the concrete.

The concrete material model itself can only be used to define the yield criterion of the material. To simulate UHPFRC behaviour a linear elastic model and a post-crack model must be implemented. Any type of linear elastic model can be used, but for describing the post-yield behaviour only a few models are applicable. The most common, and what is used in this study, is the Drucker-Prager plasticity model. This model allows a flow rule to be defined via the angle of dilatancy. The main drawback of the model is that the hardening rule is fixed to be of an elasto-plastic type.

The SOLID65 elements can have smeared reinforcement across their volume. This can, tentatively, be used to model the fibre reinforcement explicitly. The challenge is to adequately define a material model that can simulate the behaviour of the fibres. The definition requires determination of several variables that are controlled by the rheological properties of the fresh concrete, the casting procedures, the casting mould geometry and the characteristics of the fibres.

Two reference UHPFRC beams, with and without shear reinforcement, are modelled in ANSYS. They are used to study the effect of combining the built-in concrete model in ANSYS with the Drucker-Prager plasticity model. The contribution to strength and ductility from fibres are assumed to be an inherent quality of the UHPFRC. In this study, this implies that the fibres are assumed to be uniformly packed and oriented.

Experimental data on the beams are drawn from research done by Kamal et. al. (2013).

The first tests in ANSYS are performed with the built-in concrete material model alone. The results show that the model can predict the behaviour of small UHPFRC beams with shear- and longitudinal reinforcement. Without the shear reinforcement, it becomes evident that the model overestimates the shear strength of the material.

Discrepancies are found between the simulated post-crack behaviour of the concrete and the experimental data. This behaviour is the key to utilise the material to its full potential. The benefit of accurately modelling the post-crack behaviour of UHPFRC, and thereby the fibre reinforcement, is that structures made with the material can be designed with lesser amount of normal reinforcement.

Adding the Drucker-Prager plasticity model to the built-in concrete model in ANSYS, improves the accuracy of the post-crack characteristics of the UHPFRC model. To further increase the accuracy of the models, a hardening rule must be defined. This will allow analysis of UHPFRC beams in ANSYS. The built-in concrete model and the Drucker-Prager plasticity model are found to be too inflexible in this regard.

The benefit of using the concrete model and the SOLID65 element type is their ability to simulate cracking of the concrete material. They can still be used, if an appropriate model for fibre reinforcement is implemented.

10 Recommendations

Based on the work in this thesis we recommend study of the non-linear behaviour of UHPFRC with plasticity models. Alternatives to the built-in concrete model in ANSYS should be sought.

We would recommend FEM analysis of locally produced UHPFRC beams with defined characteristics where extensive test data is available. The opportunity to test the beams yourselves will allow specific test data to be collected.

11 References

[1] J. P. R. G. Christian Bøgh Jøns Nielsen, "Slanke konstruktioners potentiale i infra-strukturen," teknologisk institut DK, Taastrup, 2014.

[2] M. I. H. e. al., "Experimental study and comparison between the use of natural and artificial coarse aggregate in concrete mixture," Elsevier Ltd., Beirut, 2017.

[3] AFNOR.org, "NF P 18-710, Concrete - National addition to Eurocode 2 - Design of concrete structures: specific rules for Ultra-High Performance Fibre-Reinforced Concrete (UHPFRC)," AFNOR - French standard institute, Paris, 2016.

[4] Standard Norge, "NS-EN 1992-1-1:2004+NA:2008, Eurokode 2: Prosjektering av betongkonstruksjoner," Standard Norge.

[5] AFNOR.org, "NF P 18-470 Concrete - Ultra-High performance Fibre-Reinforced Concrete - specifications, performance, production and conformity," AFNOR - French standard institute, Paris, 2016.

[6] J. Ma, M. Orgass, F. Dehn, D. Schmidt and N. V. Tue, "Comparative Investigations on Ultra-High Performance Concrete with and without Coarse Aggregates," 2004.

[7] B. Graybeal, "Material Property Characterization of Ultra-High Performance Concrete," FHWA, U.S. Department of Transportation, 2006.

[8] Federal Highway Administration, "Ultra-High Performance Concrete: A State-of-the-Art Report for the Bridge Community," Georgetown Pike, McLean, 2013.

[9] M. Curbach and K. Speck, "Zweiaxiale Druckfestigkeit von ultrahochfestem Beton," *Beton- und Stahlbetonbau,* vol. 102, no. 10, pp. 664-673, 2007.

[10] E. V. Sarmiento, "Flowable fibre-reinforced concrete for structural applications," NTNU, Trondheim, 2015.

[11] S. Grünewald, "PERFORMANCE-BASED DESIGN OF SELF-COMPACTING FIBRE REINFORCED CONCRETE," Delft University Press, Delft, 2004.

[12] W. J. M. Rankine, "On the Stability of Loose Earth," 1857.

[13] D. Drucker and W. Prager, "Soil Mechanics and plastic analysis or limit design," 1951.

[14] A. Z. Joseph F. Labuz, Mohr-Coulomb Failure Criterion, Springer-Verlag, 2012.

[15] K. J. William and E. Warnke, "Constitutive model for the triaxial behaviour of concrete," in *Concrete structures subjected to triaxial stress*, Bergamo, Italy, 1974.

[16] D. C. Drucker, "A definition of stable inelastic material," 1957.

[17] *ANSYS 18.2 Academic Teaching Introductory, documentation embedded in the software,* 2017.

[18] D. Kachlakev and T. Miller, "Finite Element Modeling of Reinforced Concrete Structures Strengthened with FRP Laminates," 2001.

[19] M. Kamal, M. Safan, Z.A.Etman and R. Salama, "Behavior and strength of beams cast with ultra high performance concrete containing different types of fibres," *HBRC Journal,* pp. 55-63, 2014.

[20] I. Yang, C. Joh and B.S.Kim, "Flexural strength of ultra high strength concrete beams reinforced with steel fibers," in *The Twelfth East Asia-Pacific Conference on Structural Engineering and Construction*, 2011.

[21] P. Máca, R. Sovják and T. Vavřiník, "Experimental Investigation of Mechanical Properties of UHPFRC," in *Concrete and Concrete Structures 2013 Conference*, 2013.

[22] R. Zagon and K. Zoltan, "Shear Behaviour of UHPC Concrete Beams," in *9th International Conference Interdisciplinarity in Engineering*, Tirgu-Mures, Romania, 2015.

[23] A. L. Hoang and E. Fehling, "Influence of steel fiber content and aspect ratio on the uniaxial tensile and compressive behavior of ultra high perdormance concrete," *Construction and Building Materials,* vol. 153, no. October, pp. 790-806, 2017.